Received: 11 November 2020 | Revised: 22 February 2021 | Accepted: 23 February 2021

DOI: 10.1002/esp.5107

RESEARCH ARTICLE

ESPL WILEY

Modelling the response of a double-barred sandy beach system to time-varying wave angles

A. Nnafie | A.S. Driessen | H.E. de Swart | T.D. Price

Institute for Marine and Atmospheric Research, Utrecht University, The Netherlands

Correspondence
A. Nnafie, Institute for Marine and Atmospheric Research, Utrecht University, the Netherlands.
Email: a.nnafie@uu.nl

Summary

Sandy beaches typically have one or more shore-parallel bars with superimposed smaller-scale three-dimensional (3D) bars. Knowledge of their morphodynamic behaviour under more realistic wave conditions is limited. This study investigates the response of beaches with two shore-parallel bars to sinusoidally time-varying angles of incidence, using a non-linear morphodynamic model. Different periods and amplitudes of this sinusoidal variation are considered, as well as different time-mean wave angles. For time-invariant and normally incident waves, results show that alongshore rhythmic 3D bars form in the domains of inner and outer shore-parallel bars. The 3D bars in the inner domain are coupled at half the outer-bars wavelength. This phase coupling breaks up when the wave angle varies in time. Initially, regular 3D bars form in the inner domain (free behaviour), which become irregular when 3D bars develop in the outer domain (forced behaviour). The heights of the 3D bars oscillate with time, reaching maximum values when the forcing period is comparable to the system adjustment time scale (~ 10–20 days). For a time-varying wave angle around an oblique mean, alongshore migrating 3D bars emerge in both inner and outer domains. In contrast, for an oblique (constant) wave angle, 3D bars only form in the inner domain and they hardly migrate alongshore. For any forcing period, the dominant response period of the oscillating bar heights is at half the forcing period when waves are (on average) normally incident, and it equals the forcing period when waves are on average obliquely incident. Compared with time-invariant angles, heights of inner and outer 3D bars are (on average) smaller and larger, respectively, when the angle varies with time, particularly for forcing periods in the order of the system adjustment time scale. Increasing the amplitude of the time-varying wave angle weakens bar growth. Explanations of these results are also provided.

KEYWORDS
3D bars, Double-barred beach, normal and oblique mean wave angle, oscillating heights, phase coupling break-up, resonance, time-varying wave angle

1 | INTRODUCTION

Many uninterrupted sandy beaches are fronted by one or more nearshore sandbars that display a range of morphological configurations, varying from shore-parallel, straight bars (Figure 1, panel a) to bars that have alongshore rhythmic alternations in both their cross-shore position and depth (panel b), such as crescentic bars and transverse bars (Jackson & Short, 2020; Wright & Short, 1984). These alongshore-rhythmic bars (hereafter referred to as 3D bars or bars) often develop from initially straight bars. Typically, 3D bars exhibit

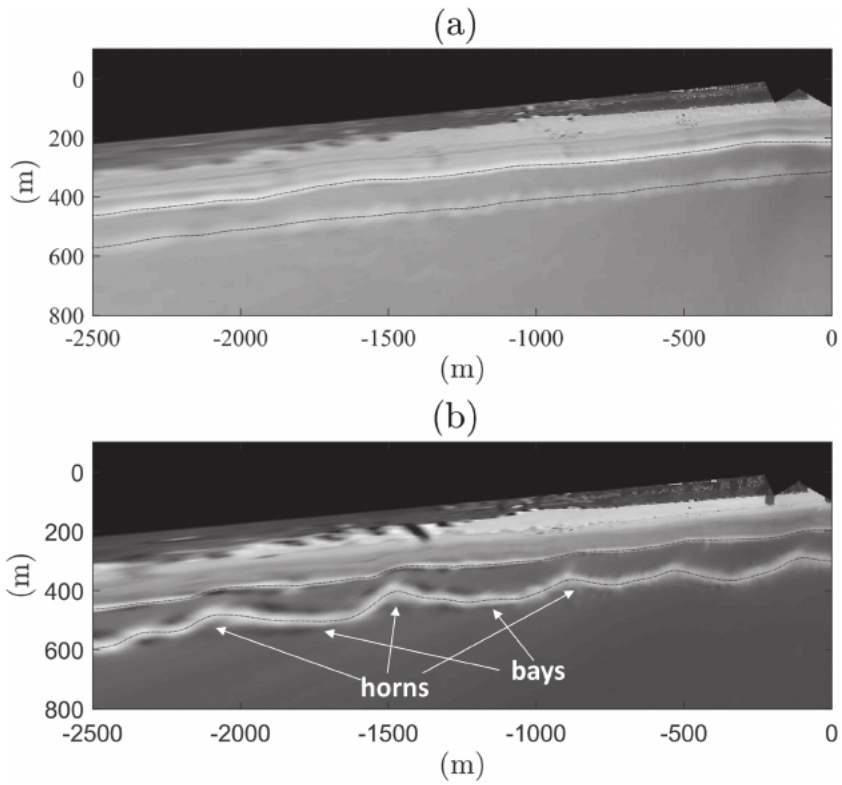

FIGURE 1 Examples of two shore-parallel bars without (a) and with (b) superimposed 3D bars

alongshore meandering sequences of shallow horns and deep bays (Figure 1b), with length scales ranging between 100 and 1000 m (Ribas et al., 2015; van Enckevort et al., 2004). Understanding the dynamics of these bars is important because they strongly influence the surf-zone hydrodynamics and the shape of the coastline (Komar, 1998; Lippmann & Holman, 1990).

The dynamics of beaches with one or two shore-parallel bars (called single- and double-barred beaches, respectively) have been extensively studied (Wright & Short, 1984; Lippmann & Holman, 1990). The initial formation of 3D bars on single-barred beaches was first studied by Deigaard et al. (1999) and Calvete et al. (2005, 2007). Other studies by for example Garnier et al. (2006, 2008, 2013) employed non-linear numerical models to study the long-term evolution (order weeks to months) of 3D bars subject to constant wave forcing. It was found that normally incident waves favour the formation of 3D bars and that their growth becomes weaker for more oblique waves. No bars form if the wave angle exceeds a critical value.

The response of a single-barred beach to time-varying wave conditions was first studied by Castelle and Ruessink (2011). They considered waves with sinusoidal variations in height, period and angle of incidence, respectively. In all their experiments, on average the waves were shore-normal. Their main findings were that time-varying forcing affects the longshore spacing of the bars and that their horns and bays are less developed, but more alongshore variable, compared with the case of a time-invariant forcing. Nnafie et al. (2020) extended this to the case of time-varying wave forcing where on average the waves are obliquely incident. They found that, depending on the mean angle of wave incidence, the mean height and migration speed of the bars could be either larger or smaller than the values obtained for a time-invariant wave forcing.

At double-barred beaches, with a more offshore-positioned outer bar and a more onshore-positioned inner bar, the initial formation of 3D bars for constant wave forcing was modelled by Klein and Schuttelaars (2006) and Coco et al. (2020), while their non-linear dynamics was addressed in the modelling studies by (Castelle et al., 2010b; Smit et al., 2008; Thiebot et al., 2012) and Price et al. (2013). Moreover, a conceptual beach state model for this type of beaches was presented in Price et al. (2014). All these studies reveal that the initial and long-term evolution of 3D bars strongly depends on both wave characteristics, as well as on the locations and depths of the inner and outer shore-parallel bar. Here, the outer bar affects the wave field (through wave breaking and wave focussing) that reaches the inner bar and, as such, may act as a template for the morphology of the inner bar (Castelle et al. 2010b). The morphodynamic evolution of the inner bar is thus governed by a mixture of self-organisation and outer-inner bar coupling mechanisms (Castelle et al., 2010b, 2010a; Price & Ruessink, 2013). Using a non-linear morphodynamic model, Castelle et al. (2010b) were able to successfully reproduce different types of phase couplings that are sometimes observed in the field (Castelle et al., 2007; Price et al., 2014; van Enckevort & Wijnberg, 1999): (1) outer-bar horns persistently face inner-bar horns (in-phase coupling), (2) outer-bar horns face inner-bar bays (out-of-phase coupling) and (3) two inner-bar rip channels occur within one outer-bar crescent (coupling at half the outer-bar wavelength, hereafter also referred to as phase-locked coupling). A major limitation in the modelling studies on double-barred beaches is that they assume constant wave forcing (constant wave height, wave period, wave angle, etc.), whereas in reality, this forcing changes continuously with time. Therefore, knowledge of double-barred beach morphodynamics under more realistic wave conditions is still lacking.

The preceding considerations motivated the overall aim of this study, that is, to gain further understanding of the morphodynamic response of a double-barred beach system to sinusoidally time-varying wave angles. In particular, the sensitivity of the height of 3D

bars, their alongshore migration speed and the longshore spacing between successive bars will be investigated for different amplitudes and periods of the forcing and different time-mean wave angles. For this, simulations were carried out with a non-linear morphodynamic model. Both the model and methodology are described in section 2. Results are presented in section 3, followed by a discussion in section 4 and the conclusions in section 5.

2 | MATERIALS AND METHODS

2.1 | Model

The non-linear morphodynamic model Morfo55 (Garnier et al. 2008) was used to study the evolution of the double-barred beach system. This numerical model solves the phase-averaged equations for waves that are characterised by a narrow frequency-direction spectrum, together with the depth-averaged shallow water equations for currents, sediment transport due to the joint action of waves and currents (formulation of Soulsby & van Rijn, is used, see Soulsby, 1997) and the Exner equation that describes the changes in the bed due to convergence and divergence of sediment transport. The Morfo55 model thus includes fully detailed wave-topography feedbacks, wave shoaling and refraction, wave breaking and wave radiation stresses. An overview of the model equations is presented in the Supporting Information (SI).

The equations of motion are solved on a rectangular domain that is bounded by the lines $x = 0$, $y = 0$, $x = L_x$ and $y = L_y$ (Figure 2). Here, the x- and y-axis point in the cross-shore direction and longshore direction, respectively, and $x = 0$ is the location of the (straight) coast in the absence of motion. The z-axis points vertically upwards, with $z = 0$ being the still-water level.

It is assumed that the beach system has an equilibrium bed profile $z = z_b^0(x)$ that represents two shore-parallel bars (dashed line in Figure 2). For this, the profile given by Yu and Slinn (2003) was extended to a double-barred beach system, resulting in

$$z_b^0 = -a_0 - a_1\left(1 - \frac{\beta_2}{\beta_1}\right)\tanh\left(\frac{\beta_1}{a_1}x\right) - \beta_2 x + c_1 e^{-w_1\left(\frac{x-x_1}{x_1}\right)^2} + c_2 e^{-w_2\left(\frac{x-x_2}{x_2}\right)^2}. \quad (1)$$

In this expression, a_0 is the depth at the coastal boundary, a_1 determines how the slope of the profile without the shore-parallel bars varies in the cross-shore direction, with β_1 and β_2 being the slopes of the nearshore part and the seaward part of the unbarred beach profile. The amplitudes of uniform, shore-parallel inner and outer bars are labelled as c_1 and c_2, respectively. Furthermore, w_1 and w_2 denote the width of the inner and outer shore-parallel bars and their positions with respect to the coast are represented by x_1 and x_2.

The actual bed level $z = z_b$, denoted by the solid line in Figure 2, is the result of convergence of sand transport and depends on both x, y and time t. The difference between the actual and the averaged bed level is defined as $h = z_b - z_b^0$. As such, bottom perturbations h represent the 3D bar morphology.

Periodic boundary conditions are imposed at the lateral boundaries ($y = 0, L_y$) and vanishing cross-shore (u) and longshore (v) velocity are assumed at the coast ($x = 0$). At the offshore boundary $x = L_x$, the model is forced by waves with constant wave peak period T_p, a root-mean square wave height H_{rms} and a time-varying angle of incidence $\theta(t)$ (Figure 2), which varies according

$$\theta(t) = \hat{\theta}\sin\left(\frac{2\pi t}{T}\right) + \theta_0, \quad (2)$$

with θ_0 the time-mean angle of incidence, $\hat{\theta}$ the amplitude of the variation in the angle and T the period of this variation.

The equations of motion are numerically solved on a staggered grid, with grid sizes Δx and Δy in the x- and y-direction, respectively. The time integration is performed by a second-order Adams–Bashforth scheme (Bashforth & Adams, 1883). In the bed evolution equation, the time step Δt is increased by a morphological acceleration factor *moac* to speed up the computations. This can be done because the time scale of morphological evolution (order of weeks) is much longer than the hydrodynamic time scale (about 1 day).

2.2 | Methods

For the model simulations, a domain was chosen that crudely mimics the double-barred beach of the Gold Coast, Australia (Price et al., 2013). The domain was set to $0 < x < L_x$ with L_x = 250 m and $0 < y < L_y$ with L_y = 1500 m. This domain was chosen such that both shore-parallel bars were fully inside the domain and that, in the longshore direction, multiple alternating horns and bays could be simulated. The parameters in Equation (1) were tuned such that initial

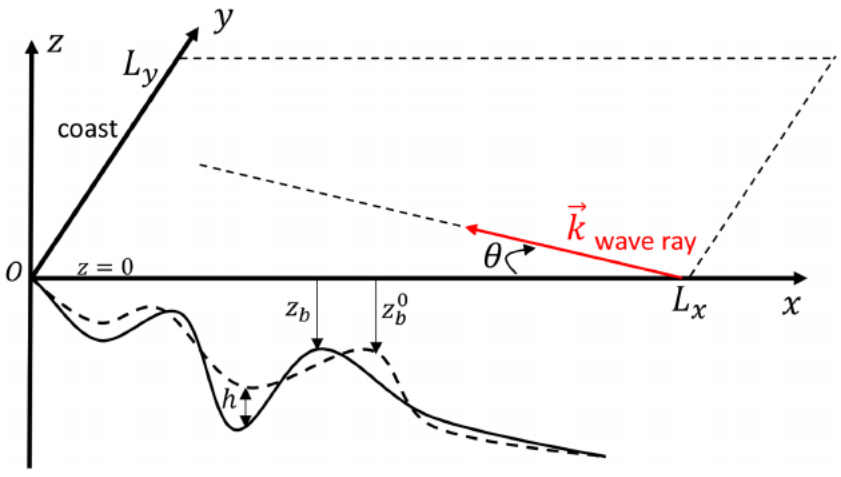

FIGURE 2 Computational domain of Morfo55 model used to study the evolution of a double-barred beach system. A Cartesian coordinate system is used, with x the cross-shore coordinate, y the longshore coordinate and z the vertical coordinate. The domain has boundaries $x = 0$, $x = L_x$, $y = 0$ and $y = L_y$. The dashed line is the initial bed level (z_b^0), the solid line is the actual bed level (z_b). Bottom perturbations (h) are the differences between the two bed levels. Furthermore, θ is the angle of incidence of the waves (with wavenumber $\vec{k}$) at the offshore boundary with respect to the shore-normal (positive clockwise) [Color figure can be viewed at wileyonlinelibrary.com]

bed profile z_b^0 resembles that of the Gold Coast beach (Price et al., 2013). A list of important physical and numerical model parameters and their values is given in Table 1. Values of other physical parameters (e.g. a grain size of 0.25 mm) are identical to those in Garnier et al. (2008) and are not explicitly given here.

To meet the objectives of this study, a number of simulations were conducted; they are named and described in Table 2. The first set of them, denoted as Run1–Runs4T, considers waves that are on average normally incident to the coast ($\theta_0 = 0^\circ$). Run1, which has constant normal incidence ($\theta(t) = 0^\circ$), is the reference case of this set of simulations. Runs2T are simulations with sinusoidally time-varying angles around 0°, having an amplitude of $\hat{\theta} = 3^\circ$ and different periods, $T = 2.5, 5, 7.5, 10, 15, 20$ and 25 days. These simulations were repeated for higher amplitudes of the variation in the wave angle, $\hat{\theta} = 6^\circ$ (Runs3T) and $\hat{\theta} = 9^\circ$ (Runs4T).

The second set of simulations (Run5–Runs8T) has the same design as the first set, the main difference being that, on average, the waves at the offshore boundary are obliquely incident to the coast, that is, $\theta_0 = 4^\circ$. Run5 assumes constant obliquely incident waves ($\theta(t) = 4^\circ$), which is the reference run for this particular set. Runs6T have sinusoidally varying angles of incidence around a mean angle $\theta_0 = 4^\circ$, an amplitude $\hat{\theta} = 3^\circ$ and periods $T = 2.5, 5, 7.5, 10, 15, 20$ and 25 days. These series were repeated for amplitudes $\hat{\theta} = 6^\circ$ and $\hat{\theta} = 9^\circ$, Runs7T and Runs8T, respectively.

In all the simulations, random bottom perturbations ('white noise') with an amplitude of 2.5 cm were superimposed on the initial bathymetry to trigger the self-organisation processes. The simulations were run for a maximum time period of 125 days.

TABLE 1 List of physical and numerical model parameters

Symbol	description	value
Domain		
L_x	cross-shore domain length	250 m
L_y	longshore domain length	1500 m
Profile		
a_0	depth at coastal boundary	0.25 m
a_1	shape parameter	2.97
β_1	slope first part bottom	0.034
β_2	slope of second part bottom	0.0245
c_1	amplitude inner bar	0.8 m
c_2	amplitude outer bar	2.36 m
x_1	position inner bar	40 m
x_2	position outer bar	140 m
w_1	width inner bar	20 m
w_2	width outer bar	40 m
Hydrodynamics		
T_p	wave peak period at offshore boundary	9 s
H_{rms}	root-mean-square wave height	1.5 m
Numerics		
Δx	cross-shore grid size	5 m
Δy	longshore grid size	20 m
Δt	time step	0.05 s
moac	morphological acceleration factor	90

Note: The left, middle and right column list the symbols used in this study, a short description of their meanings and their values that are used in the simulations, respectively. Other model parameter values are identical to those in Garnier et al. (2008).

2.3 | Presentation and analysis of model output

Besides showing snapshots of the actual bed level $z = z_b(x, y, t)$ and of the bottom perturbations $h = z_b - z_b^0$ at different times, the alongshore and temporal behaviour of h will be shown along two longshore transects ($x = x_t$) at the offshore locations of the inner and outer shore-parallel bars: $x_t = x_1 = 40$ m and $x_t = x_2 = 140$ m. In addition, the longshore dominant spacings λ_d of the 3D bars that develop near the inner and outer shore-parallel bars are analysed. To this end, the discrete Fourier transform of bottom perturbations h are computed along the two longshore transects $x_t = 40, 140$ m:

$$F(x_t, k_l, t) = \sum_{j=1}^{N_y} h(x_t, y_j) e^{-i\frac{2\pi}{N_y}(j-1)(l-1)}, \quad k_l = \frac{2\pi(l-1)}{L_y}, l = 1 : N_y, y_j = j\Delta y. \tag{3}$$

Here, $F(x_t, k_l, t)$ is the Fourier coefficient that corresponds to the topographic wavenumber k_l and N_y is the number of grid points in the longshore direction (y). The wavenumber for which the modulus of the Fourier coefficient ($|F(x_t, k_l, t)|$) is maximum for a given time t and longshore position x_t defines the dominant mode, which is used to compute the longshore dominant spacing λ_d.

Furthermore, extending Garnier et al. (2006), a root-mean-square (rms) height ($||h||$) of the 3D bars is defined in two different subdomains:

$$||h||_i = \left(\frac{1}{x_h L_y} \int_0^{L_y} \int_0^{x_h} h^2 dx\, dy \right)^{1/2}, \tag{4}$$

$$||h||_o = \left(\frac{1}{(L_x - x_h) L_y} \int_0^{L_y} \int_{x_h}^{L_x} h^2 dx\, dy \right)^{1/2}. \tag{5}$$

TABLE 2 List of runs conducted in this study

Run name	Description
Run1	$\theta(t) = \theta_0 = 0^\circ$.
Runs2T	$[\theta_0, \hat{\theta}] = [0, 3]^\circ$, $T = [2.5, 5, 7.5, 10, 15, 20, 25]$ days.
Runs3T	$[\theta_0, \hat{\theta}] = [0, 6]^\circ$, $T = [2.5, 5, 7.5, 10, 15, 20, 25]$ days.
Runs4T	$[\theta_0, \hat{\theta}] = [0, 9]^\circ$, $T = [2.5, 5, 7.5, 10, 15, 20, 25]$ days.
Run5	$\theta(t) = \theta_0 = 4^\circ$.
Runs6T	$[\theta_0, \hat{\theta}] = [4, 3]^\circ$, $T = [2.5, 5, 7.5, 10, 15, 20, 25]$ days.
Runs7T	$[\theta_0, \hat{\theta}] = [4, 6]^\circ$, $T = [2.5, 5, 7.5, 10, 15, 20, 25]$ days.
Runs8T	$[\theta_0, \hat{\theta}] = [4, 9]^\circ$, $T = [2.5, 5, 7.5, 10, 15, 20, 25]$ days.

Note: Here, θ_0 is the time-mean angle of incidence at the offshore boundary, $\hat{\theta}$ is the amplitude of the variation in the angle and T is the period of this variation.

Here, the boundary between the inner domain (*i*) and outer domain (*o*) is halfway between the locations of two shore-parallel bars, that is, at $x_h = 90$ m.

Finally, the temporal response of the heights of the 3D bars to the time-varying wave angle will be analysed in terms of (1) the degree of the temporal response, (2) the dominant periods that exist in this response and (3) the mean height of the bars $\langle ||h|| \rangle$. The degree of the response will be quantified by computing the standard deviation $\sigma_{||h||'}$ of the bar height anomalies $||h||'$ with respect to the time-running mean height $||h||_{rm}(t)$, that is, $||h||'(t) = ||h||(t) - ||h||_{rm}(t)$. Time-running mean height $||h||_{rm}(t)$ is obtained by a continuous averaging of $||h||$ over one oscillation period T, that is, $||h||_{rm} = (1/T)\int_{t-T}^{t} h(t')dt'$. Of particular importance here is the behaviour of bar height anomalies $||h||'$ when the forcing period T is comparable to the adjustment time scale of the double-barred beach system (T_a). Dominant response periods that exist in the temporal response of the bar heights ($T_{||h||'}$) will be retrieved from the discrete Fourier transforms of time series of height anomalies $||h||'$. Finally, mean height $\langle ||h|| \rangle$ is obtained by averaging $||h||(t)$ over a period of 70 days during the non-linear evolution of the bars.

3 | RESULTS

3.1 | Normally incident waves

3.1.1 | Constant versus time-varying wave angle

The output of the reference case with a constant angle $\theta = 0^\circ$ (Run1) is compared with that of the case with a time-varying angle with a mean angle of $\theta_0 = 0^\circ$, an amplitude $\hat{\theta} = 3^\circ$ and a period $T = 10$ days (Runs2T$_{10}$). Snapshots of the 3D bars at different times are displayed in Figure 3 (blue-white-red colourmap, represented by bottom perturbations *h*). The left column of this figure shows the results of Run1,

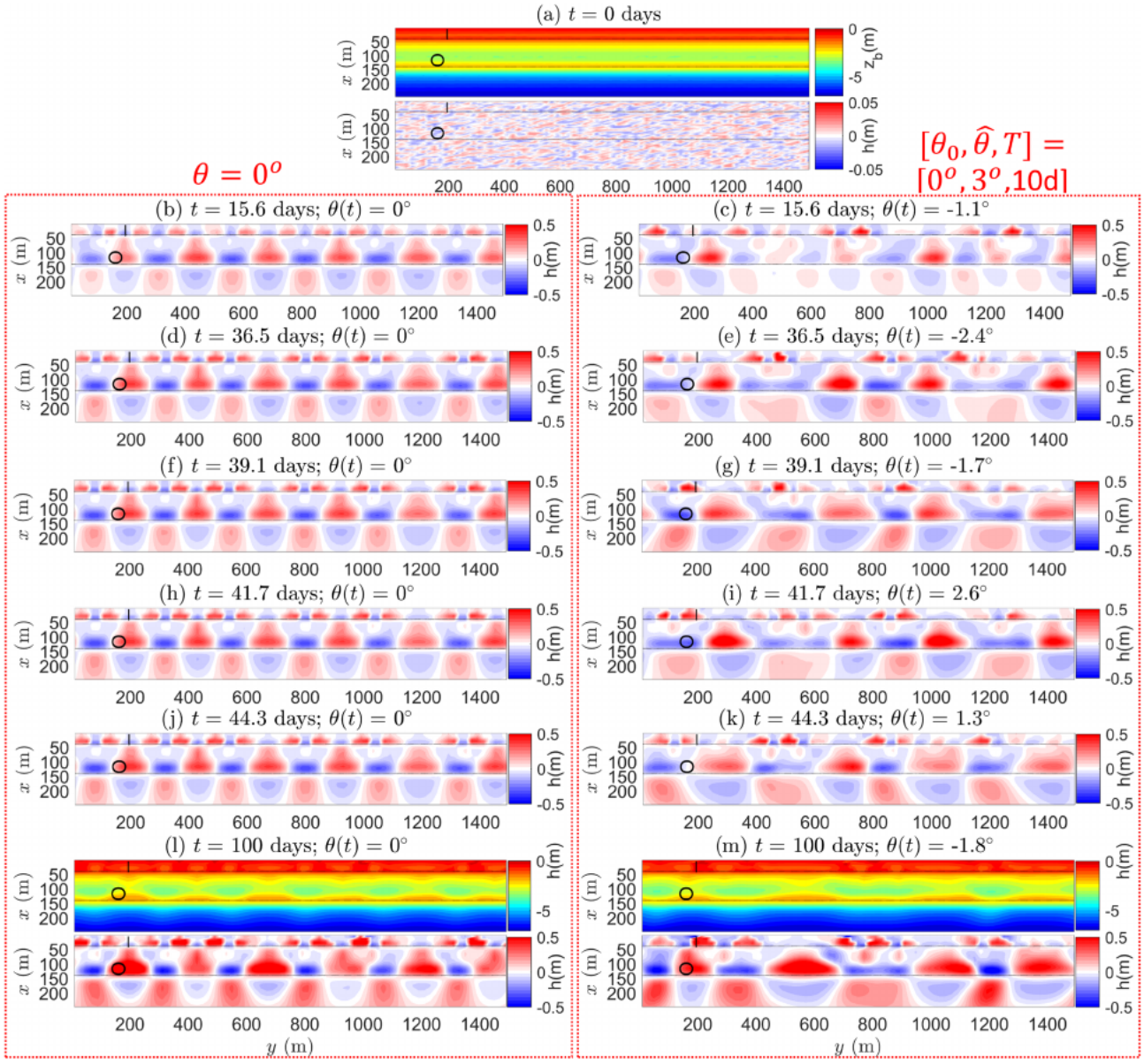

FIGURE 3 Snapshots of bottom perturbations h (blue-white-red colourmap) at different points in times in the cases of Run1 (constant angle, $\theta(t) = 0^\circ$, left columns) and Runs2T$_{10}$ ($[\theta_0, \hat{\theta}, T] = [0^\circ, 3^\circ, 10\text{d}]$, right columns). Panel a shows the initially random perturbations h ('white noise') that were superimposed on the initial bed level z_b^0 (jet colourmap). The simulated bed levels at $t = 100$ days are visualised in panels l and m. The dashed black lines denote the locations of the inner (i) and outer (o) shore-parallel bars [Color figure can be viewed at wileyonlinelibrary.com]

while the right column shows those of Run2T$_{10}$. The panels d-k cover approximately a full period of the variation in wave angle. Panel a displays bed level z_b and bottom perturbations h at $t = 0$, while panels l and m show z_b and h at $t = 100$ days.

In Run1 alongshore rhythmic 3D bars form that do not change much in time and space (Figure 3, left panels). These bottom patterns exhibit alongshore sequences of horns (red colours) and bays (blue colours) that alternate shoreward and seaward of both the initially shore-parallel inner and outer bars (indicated by the dashed lines '*i*' and '*o*' in Figure 3). The 3D bars in the outer domain have larger spatial scales than those in the inner domain. A horn in the outer domain is always faced by a bay in the inner domain, while an outer bay is faced by two inner horns with a small inner bay in between. The outer horn and inner bay are almost connected by a bulge of the outer horn toward the coast. The development of the 3D alongshore rhythmic bottom topography causes the initially straight inner and outer longshore-parallel bars (panel a, jet colourmap) to have a meandering shape (panel l). The 3D bars are rather different when there is a time variability in the wave angle, which leads to the formation of a much more irregular bottom topography. The outer horn is sometimes faced by two inner bays (panels e, g) and sometimes by an inner horn/bay (panel m). Moreover, relative to the case of the constant angle, the horns and bays are generally much wider and their shapes alternate between down-current and up-current orientations during one forcing period (panels e, g, i, k), particularly the horns/bays of the outer domain.

The regular and irregular 3D bars that develop in, respectively, the cases with constant and time-varying wave angles are also visible in Figure 4, which displays the time evolution of h along two longshore transects in the inner and outer domains (along the dashed lines '*i*' and '*o*' in Figure 3). While no longshore bar movements occur in the case of the constant angle (panels a, c), the bars of the case of the time-varying angle exhibit a rather complex development (panels b, d), particularly those that form in the inner domain. The latter migrate back and forth in the longshore direction, as a result of the changing wave angle (panel f). Moreover, merging and splitting of the inner horns and bays occur in time, features that are less pronounced in the outer domain. Figure 4 further reveals that the evolution of the inner bars becomes irregular at the time that 3D bars appear in the outer domain (around $t = 15$ days, indicated by the first vertical dashed line in Figure 4b-d). The regular and the irregular pattern formations of the cases of the constant and time-varying wave angle are also reflected in the longshore wavelengths (distance between successive horns/bays) of the 3D bars (Figure SI-1 of the Supporting Information, SI). While in the former case bars in the inner and outer domains have distinct longshore wavelengths λ_d of about 125 and 250 m, respectively, those in the latter case have no clear wavelengths. Note the transition from a sharp to a blurry

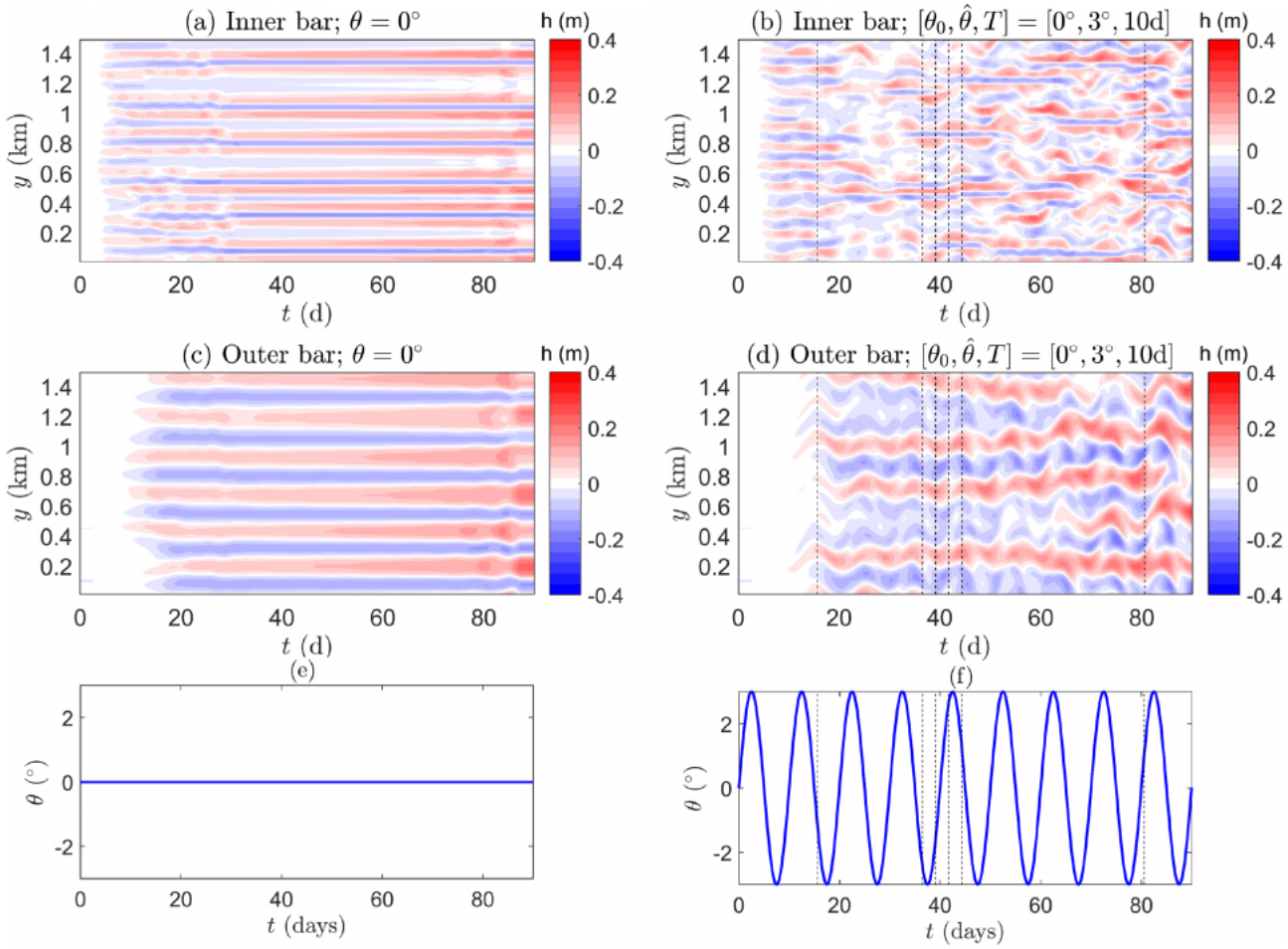

FIGURE 4 a-d) Time series of bottom perturbations along the longshore transects at $x_1 = 40$ m (h(40, y, t)) and $x_2 = 140$ m (h(140, y, t)) in the cases of Run1 (a, c) and Runs2T$_{10}$ (b, d). Offshore wave angle (θ(t)) versus time in the two cases is depicted in the bottom panels. Vertical dashed lines in the right panels indicate times at which the snapshots shown in Figure 3 were taken [Color figure can be viewed at wileyonlinelibrary.com]

wavenumber spectrum as soon as 3D bars start to develop in the outer domain (Figure SI-1, panel b).

Results further show (Figure 5a) that, in both the cases of constant (black lines) and time-varying (red lines) wave angle, the 3D bars undergo an initial stage of rapid growth and a subsequent stage of non-linear evolution, without any tendency towards saturation. This ultimately leads to model blow-up (horizontal lines). Relative to the case of the constant angle (solid black line), 3D bars in the outer domain start to grow several days later in the case of the time-varying wave angle (dashed black line). Moreover, once mature bars develop, their rms heights $||h||$ oscillate in time, meaning that these bars experience alternating periods of growth and decay. On average, the inner bars are lower and the outer bars have approximately the same height when compared with those of the time-invariant angle. Height anomalies $||h||'$ of the inner and outer bars have standard deviations $\sigma_{||h||'}$ of ~0.01 m and ~0.02 m, respectively (panel b). Time series of these anomalies have a dominant period $T_{||h||'} = 5$ days (panel c), meaning that the response period is half the forcing period, that is, $T_{||h||'} = \frac{1}{2}T$.

3.1.2 | Sensitivity to different forcing periods

Simulations were also done for time-varying wave angles with different periods T (Runs2T, $T = 2.5, 5, 7.5, 15, 20, 25$ days). Also in these cases, the 3D bars that develop in both the inner and outer domains behave similarly as those of $Run2T_{10}$ (see Figure SI-2 of the SI). Initially, bars occur only in the inner domain, which exhibit a regular morphodynamic evolution. However, as soon as there is morphodynamic activity in the outer domain (about 5 to 10 days later), the 3D bottom topography becomes irregular. Merging and splitting of horns/bays occur several times, especially those in the inner domain. Moreover, the longshore movements of inner bays/horns seem to follow those of the outer ones, a feature that is more pronounced for a large forcing period of the wave angle (Figure SI-2). These results once more indicate that as soon as mature bars develop in the outer domain, the evolution of the inner bars undergoes a transition from a free to a forced behaviour.

In all cases with different periods T, mean heights $\langle||h||\rangle$ of the 3D bars in the inner domain are smaller than those of the case of a constant angle ($\langle||h||\rangle_{\theta=0}$), especially when forcing period T is small (Figure 6(a)). With increasing T, the inner bars become higher. Compared with the case of the constant angle, mean bar height $\langle||h||\rangle$ in the outer domain is smaller for small T (2.5,5 days), approximately equal for $T = 10, 20, 25$ days and larger for $T = 7.5, 15$ days. The standard deviation ($\sigma_{||h||'}$) of height anomalies $||h||'$ tends to become larger with increasing T, particularly that of the outer bars (panel b). A peak in $\sigma_{||h||'}$ occurs around $T = 15$ days, meaning that bars experience maximum oscillations of their heights for this period. This suggests that the bar system becomes resonant for a specific forcing period. In most of the cases of different T, time series of heights anomalies $||h||'$ of the inner and outer bars have a dominant period that is half the forcing period, that is, $T_{||h||'} = \frac{1}{2}T$ (panel c). Exceptions are the small periods ($T = 2.5, 5$ days), where the time series are so distorted that no dominant response period $T_{||h||'}$ could be identified.

3.1.3 | Sensitivity to different forcing amplitudes

Results from sensitivity runs to different forcing amplitudes $\hat{\theta}$ (Runs3T and Runs4T) show that an increasing $\hat{\theta}$ weakens the growth of bottom

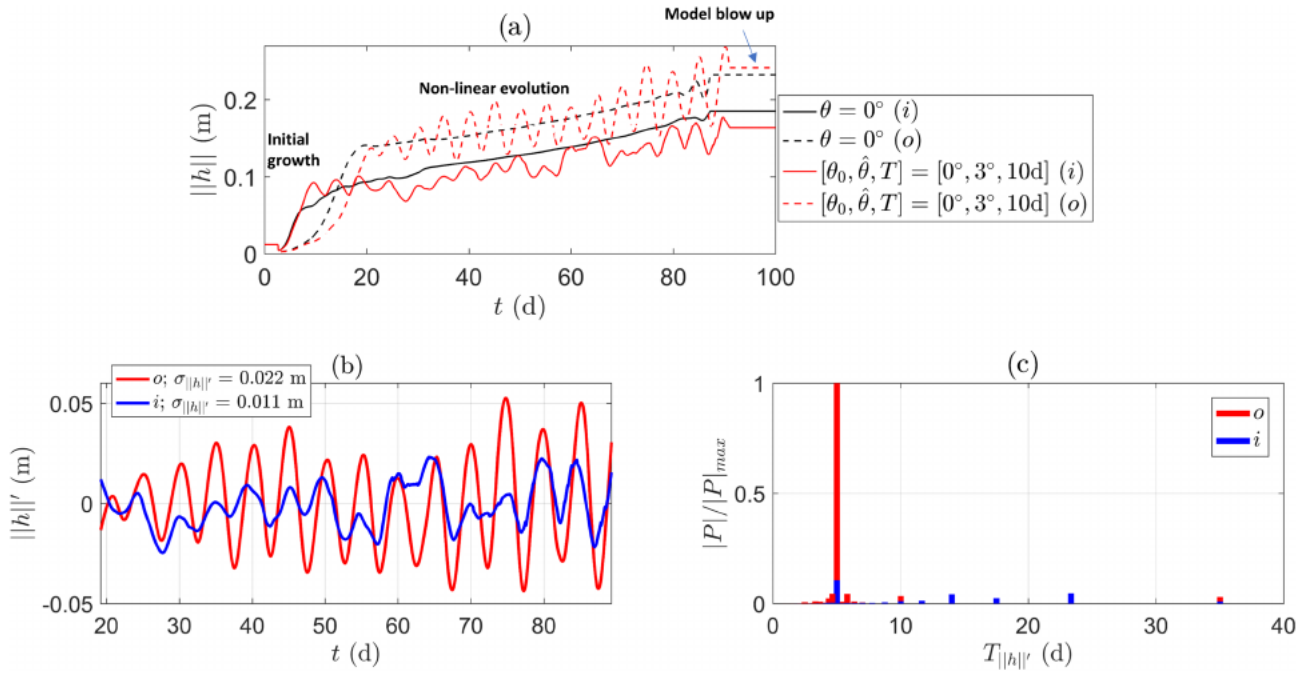

FIGURE 5 (a) Time series of the root-mean-square (rms) height ($||h||$) of the bottom perturbations that grow in inner (i) and outer (o) domains (solid and dashed lines, respectively) in cases of Run1 and $Run2T_{10}$. The 3D bars undergo an initial stage of rapid growth and a subsequent stage of non-linear evolution during which their height increases in time. This ultimately leads to model blow-up. (b) case $Run2T_{10}$: Time series of height anomalies $||h||'$ ($= ||h|| - ||h||_{rm}$) of the inner and outer bars. Running-time mean $||h||_{rm}(t)$ is obtained by a continuous averaging (over one oscillation period) of $||h||$ (panel a) during the non-linear stage. Modulus of Fourier coefficients ($|P|$) of the time series of $||h||'$ versus response period $T_{||h||'}$ (so-called periodogram) is shown in panel c. Values of $|P|$ are scaled with the maximum value ($|P|_{max}$) of the time series of $||h||'$ of the outer bars [Color figure can be viewed at wileyonlinelibrary.com]

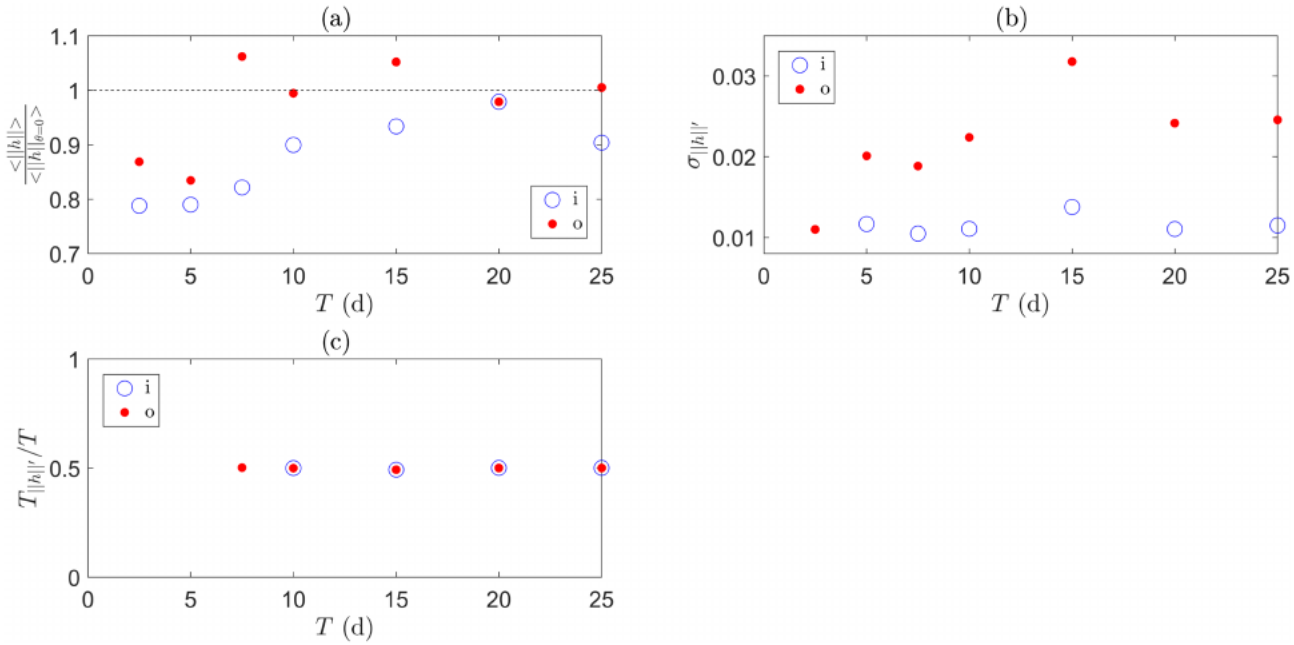

FIGURE 6 (a) Time-mean heights $\langle||h||\rangle$ of inner and outer bars (scaled with their corresponding value in the case of constant angle $\theta = 0^{\circ}$ (Run1)) for different forcing periods T (Runs2T). Mean heights $\langle||h||\rangle$ are obtained by averaging ||h|| over 70 days during the same period of the non-linear evolution of the bars (between $t = 25$ days and $t = 95$ days). (b, c) As in (a) but for the standard deviation $\sigma_{||h||'}$ and the response period $T_{||h||'}$ (scaled with T) of height anomalies $||h||'$ of the inner and outer bars. Note that no dominant response periods $T_{||h||'}$ could be identified for small periods ($T = 2.5, 5$ days) [Color figure can be viewed at wileyonlinelibrary.com]

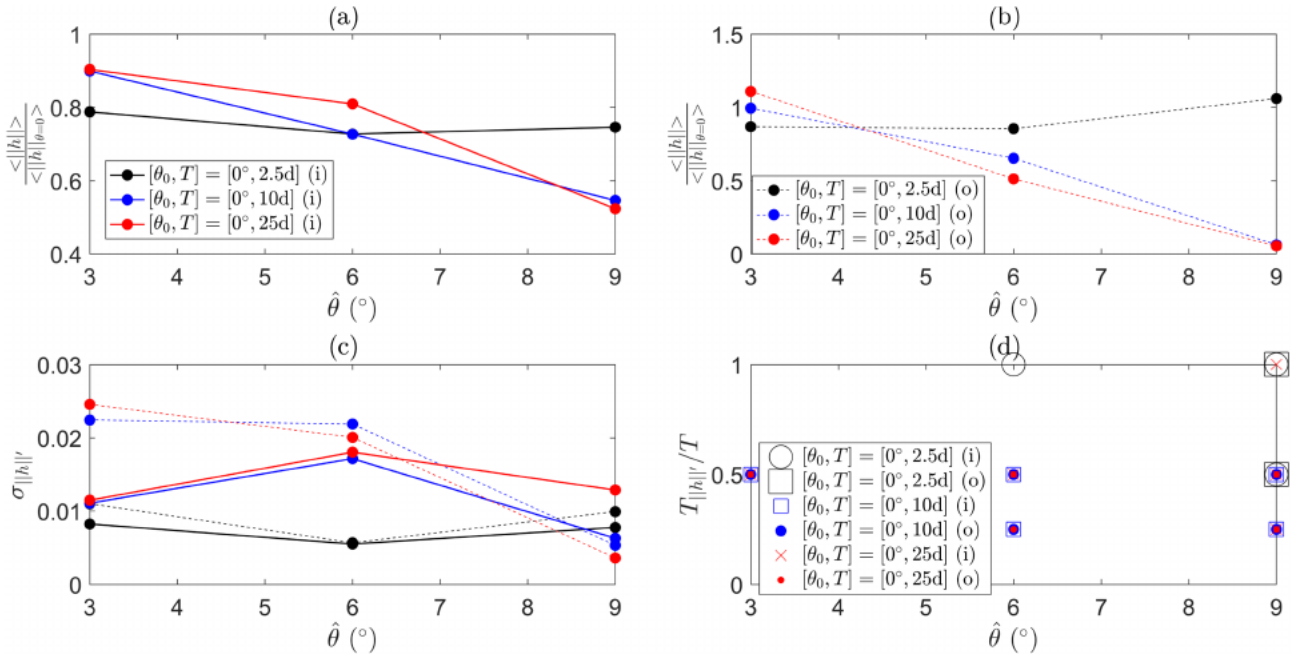

FIGURE 7 (a-b) Mean heights $\langle||h||\rangle$ of inner (a) and outer bars (b) (scaled by their corresponding value in the case of constant angle $\theta = 0^{\circ}$) for different amplitudes $\hat{\theta}$ and different forcing periods T (Runs3T and Runs4T). (c-d) As in (a-b) but for the standard deviation $\sigma_{||h||'}$ and the dominant response periods $T_{||h||'}$ of the time series of height anomalies $||h||'$. Note that the legends of panels a and b both apply to panel c [Color figure can be viewed at wileyonlinelibrary.com]

patterns when period T is sufficiently large (10–25 days, Figure 7a-b). These periods are comparable to the adjustment time scale of the system, which is in the order of 10 days, as can be seen from Figure 5a. When $\hat{\theta}$ becomes too large ($\hat{\theta} = 9^{\circ}$) and the period T is in the order of 10 days, no mature bars develop in the outer domain. The absence of bars in the outer domain leads to the formation of more regularly spaced bars in the inner domain (Figure SI-3), with a dominant longshore wavelength λ_d of about 175 m (Figure SI-4). Moreover, the height of inner bars saturates, that is, it does not increase in time during the non-linear evolution of the bars. Results further show that, when the forcing period T is comparable to the adjustment time scale of the system, the bars in the inner domain have an optimum in their height oscillation around $\hat{\theta} = 6^{\circ}$ (blue and red solid lines in Figure 7c). The most dominant response period in time series of height anomalies

$||h||'$ of the inner and outer bars does not change with increasing $\hat{\theta}$, that is, $T_{||h||'} = \frac{1}{2}T$. However, other (less dominant) response periods $\left(T_{||h||'} = [1, \frac{1}{4}]T\right)$ also appear for higher $\hat{\theta}$ (Figure 7d).

3.2 | Obliquely incident waves

3.2.1 | Constant versus time-varying wave angle

The reference simulation for the setting of a non-zero mean angle of wave incidence at the offshore boundary is Run5 (constant wave angle $\theta = 4^\circ$). Its output is compared with that of Runs6T$_{10}$ (time-varying wave angle around a mean angle $\theta_0 = 4^\circ$, having a period $T = 10$ days and amplitude $\hat{\theta} = 3^\circ$). Snapshots of bottom perturbations h (Figure 8) show that, in the case of a constant angle, bar activity in the outer domain is very low (left panels). In the case of the time-varying wave angle, 3D bars initially develop only in the inner domain, but in the course of time bars also appear in the outer domain (right panels). Alternating horns and bays form shoreward of the inner shore-parallel bar, while a (weak) mirror image of these features also develops seaward of this bar, where the 3D bars are somewhat obliquely aligned with respect to the coast. As long as there is no significant morphodynamic activity in the outer domain, the inner bars have an alongshore rhythmic structure with a dominant wavelength λ_d of $\sim$ 185 m (Figure SI-5), which is slightly larger than that of the case of the constant angle (about 160 m). This regular configuration of the inner bays/horns changes drastically when 3D bars develop in the outer domain (panel m). From Figure 9 it appears that this situation occurs around $t = 70$ days.

Figure 9 further shows that, when the wave angle of incidence is constant, the 3D bars in the inner domain do not migrate after $t \sim 20$ days (panel a). In the case of the time-varying wave angle during the stage that there are not yet 3D bars in the outer domain, the bars in the inner domain have a regular longshore migration of about

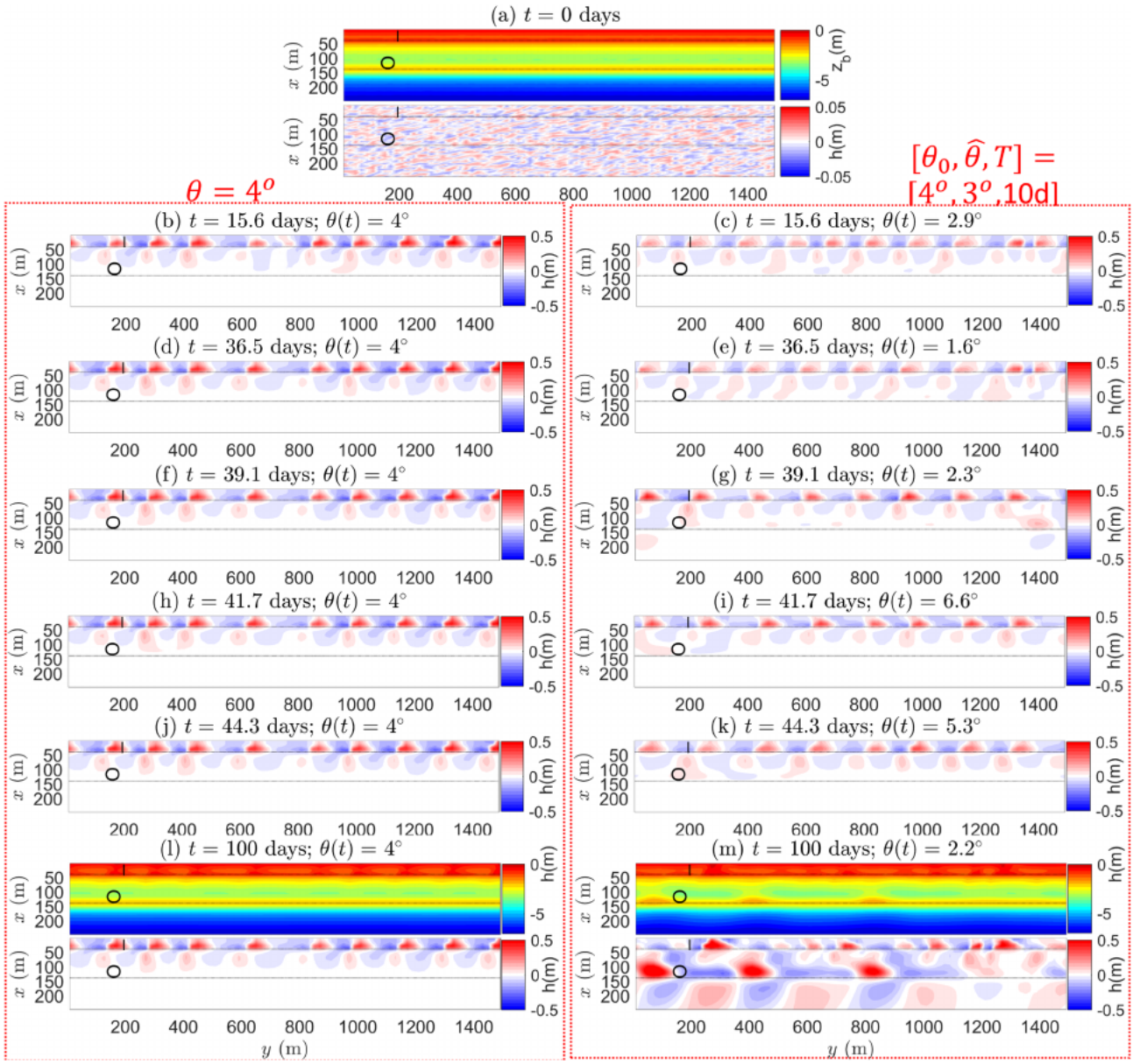

FIGURE 8 As in Figure 3, but in the cases of Run5 (constant angle, $\theta(t) = 4^\circ$, left columns) and Runs6T$_{10}$ ($[\theta_0, \hat{\theta}, T] = [4^\circ, 3^\circ, 10\text{d}]$, right columns) [Color figure can be viewed at wileyonlinelibrary.com]

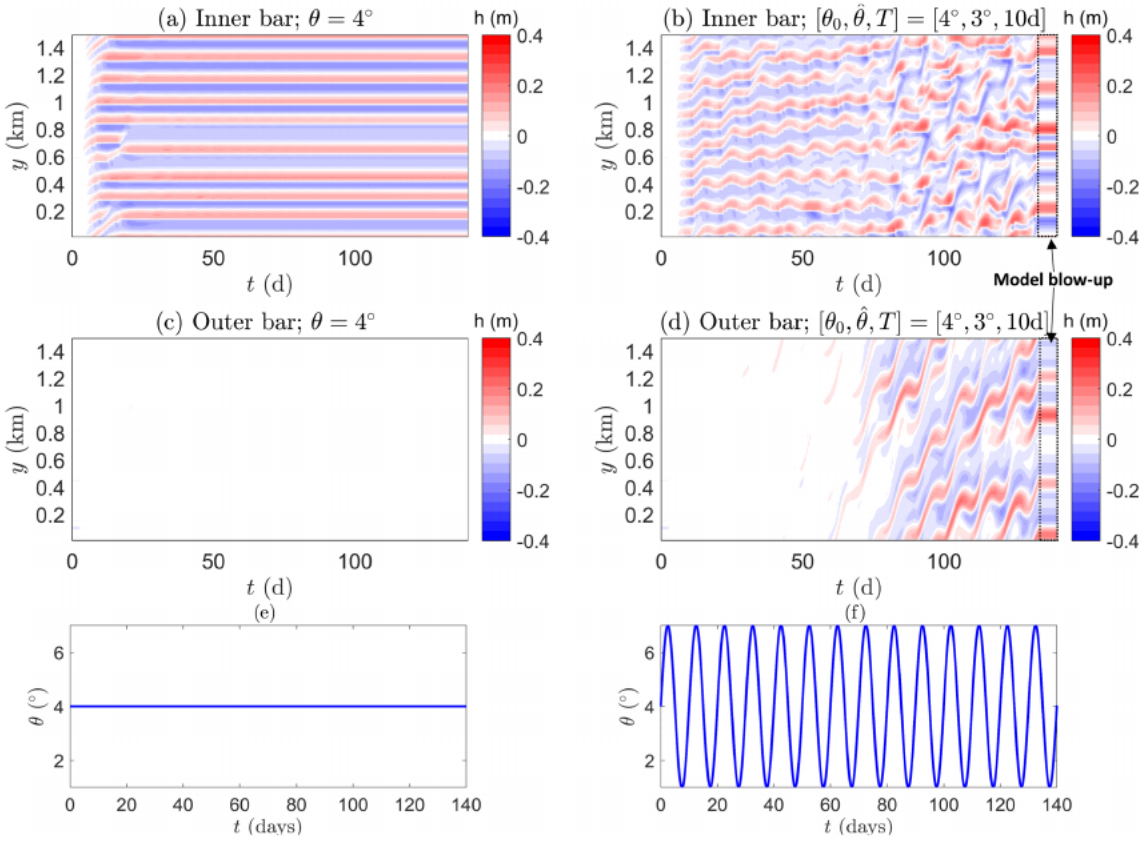

FIGURE 9 As in Figure 4, but for the cases of Run5 and Runs6T$_{10}$. Note that, due to the continuous increase of the height of the bars in panels b and d, the model blows up around t = 130 days (denoted by the rectangles) [Color figure can be viewed at wileyonlinelibrary.com]

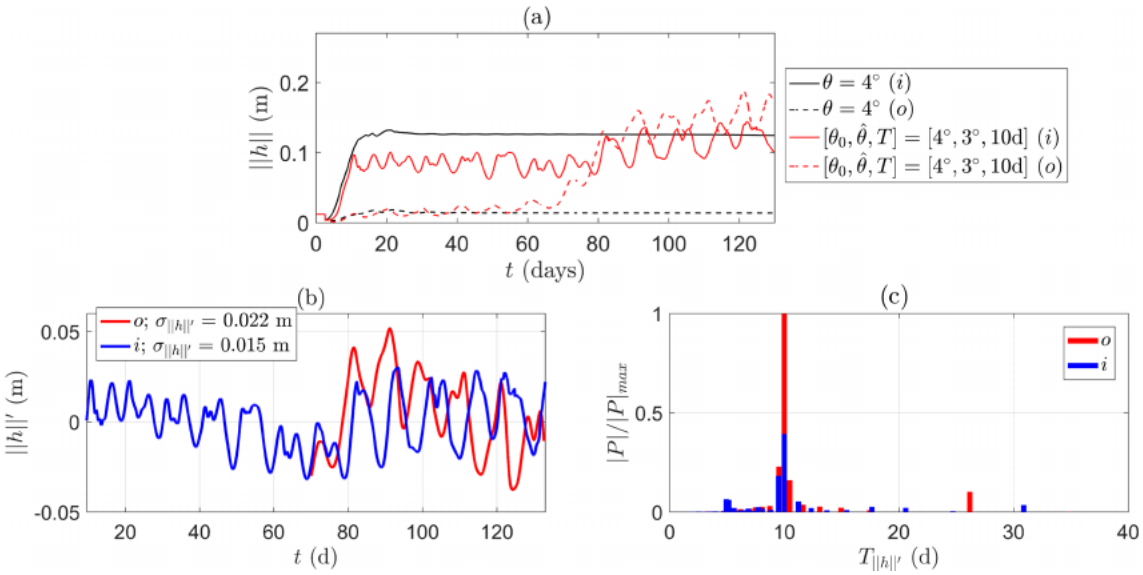

FIGURE 10 As in Figure 5, but for the cases of Run5 and Runs6T$_{10}$ [Color figure can be viewed at wileyonlinelibrary.com]

4.5 m/day in the positive y-direction (panel b). Once 3D bars form in the outer domain, the inner bars start to follow the rapidly migrating outer bars (at a rate of ~34 m/year, panel d).

Figure 10 shows that, prior to the development of 3D bars in the outer domain, the inner bars in the case of the time-varying wave angle are on average lower than those in the case of constant angle (panel a). However, once there is bar activity in the outer domain, the inner bar height starts to increase and it eventually becomes similar to that in the case of constant angle. Also, the amplitude of height anomalies $||h||'$ of the inner bars becomes similar to that of the outer bars (panel b). This is another indication of the transition of the system from a free to a forced behaviour. The time series of height anomalies $||h||'$ of the inner and outer bars have standard deviations $\sigma_{||h||'}$ of about 0.015 m and 0.022 m, respectively (panel b). These time series have a dominant response period that is equal to the forcing period, that is, $T_{||h||'} = T$ (panel c). However, there is also a less dominant

response period of half the forcing period $\left(T_{||h||'} = \frac{1}{2}T\right)$ in the time series of $||h||'$ of the inner bars.

3.2.2 | Sensitivity to different forcing periods

The 3D bars in the cases of other forcing periods (in the range $T = [2.5 - -25]$ days, Runs6T) behave similarly to those in the case when $T = 10$ days. Initially, a regular spatial pattern forms in the inner domain. In the course of time, rapidly migrating bars (with migration rates in the order of tens of meters per day) start to grow in the outer domain, which affect the growth and migration of the inner bars (Figure SI-6). Relative to the case of the constant angle, the average inner bar heights $\langle||h||\rangle$ are smaller (Figure 11, panel a), despite the height increase when bars develop in the outer domain. The standard deviation $\sigma_{||h||'}$ reaches a maximum for a forcing period $T = 20$ days. This means that the oscillations of the bar heights are strongest for this period, particularly those of the outer bars (panel b). This resonance period is larger than that in the cases of the normal mean angle ($T = 15$ days). Unlike the latter cases, where time series of height anomalies $||h||'$ have a dominant period that is half the forcing period, the dominant response period in the cases of the oblique mean angle is equal to the forcing period ($T_{||h||'} = T$). However, there is also a less dominant response period of $T_{||h||'} = \frac{1}{2}T$ in the height anomalies of the inner bars (panel c).

3.2.3 | Sensitivity to different forcing amplitudes

Results in the cases of the oblique mean angle $\hat{\theta} = 4^\circ$ and larger amplitudes $\hat{\theta}$ (Runs7T, Runs8T) are qualitatively similar to those in the cases of the normal mean angle (Runs3T, Runs4T). A quantitative difference is that larger $\hat{\theta}$ further weakens bar growth when the forcing period is comparable to the adjustment time scale of the system (order 10 days) (Figure 12a-b). For this forcing period there is hardly any morphodynamic activity in the outer domain when $\hat{\theta} > 3^\circ$. As a result, regularly longshore spaced bar patterns form in the inner domain, having distinct wavelengths λ_d of about 140 m (Figure SI-7). For forcing periods T in the order of 10 days, height anomalies $||h||'$ of the inner bars become stronger with increasing $\hat{\theta}$ (Figure 12c). This is the result of the alternating periods of disappearance and reappearance of inner bars in the course of time, which is more pronounced for large amplitudes $\hat{\theta}$ (Figure SI-8).The dominant period in the time series of height anomalies $||h||'$ does not change with increasing $\hat{\theta}$, that is, $T_{||h||'} = T$. A less dominant response period of $T_{||h||} = \frac{1}{2}T$ also occurs in these time series (Figure 12d).

4 | DISCUSSION

The main new contribution of this study is that it yields quantitative information about the morphodynamic response characteristics of a modelled double-bar beach system to waves with an angle of incidence that periodically varies in time around a mean value. It extends other model studies on the non-linear morphodynamics of double-bar beaches that considered time-invariant forcing only (Castelle et al., 2010b; Thiebot et al., 2012). Below, interpretations of several of the results presented in the previous section are given, links with field data are made and limitations of the model are discussed.

4.1 | Bed evolution equation

In order to explain the formation of 3D bottom patterns, the bottom evolution equation (Equation S9 in the SI) will be analysed. Using mass conservation of water and sediment, that is, Equations S8 and S10 in the SI, Equation S9 can be approximated as (Ribas et al., 2015)

$$(1-p)\frac{\partial h}{\partial t} \simeq -D\vec{v}\cdot\vec{\nabla}C + \vec{\nabla}\cdot(\Gamma\vec{\nabla}h), \tag{6}$$

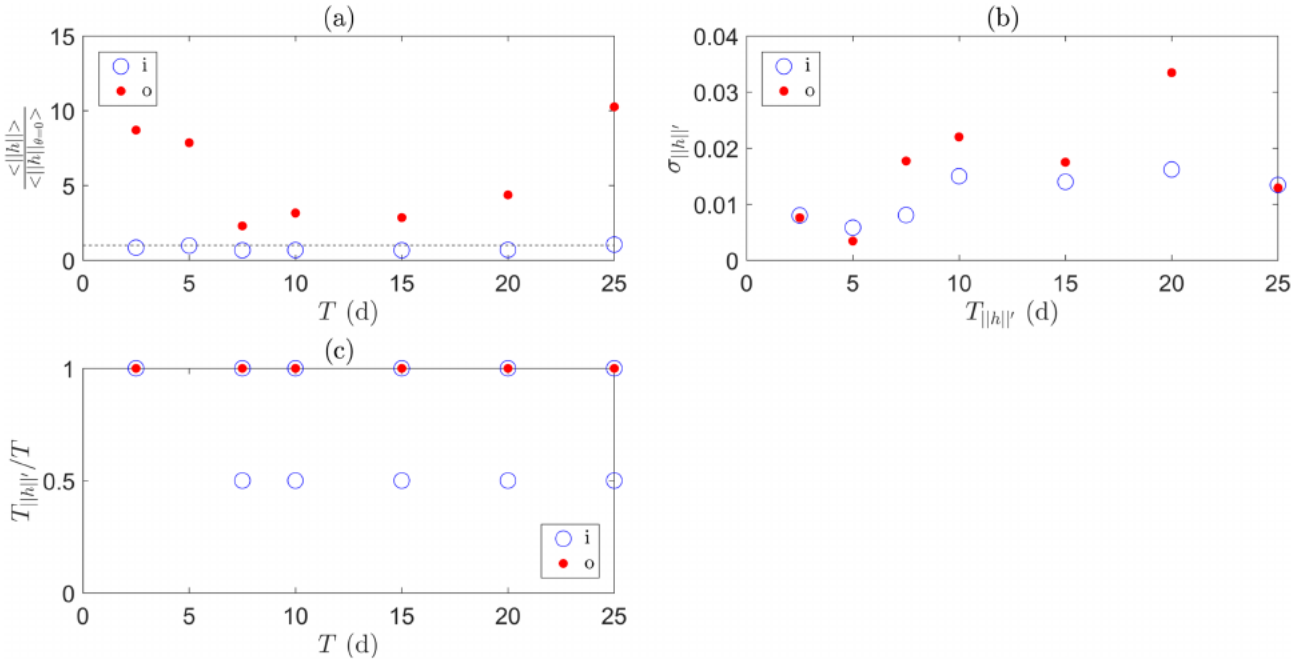

FIGURE 11 As in Figure 6, but in the cases of an oblique mean angle ($\theta_0 = 4^\circ$, Run5 and Runs6T) [Color figure can be viewed at wileyonlinelibrary.com]

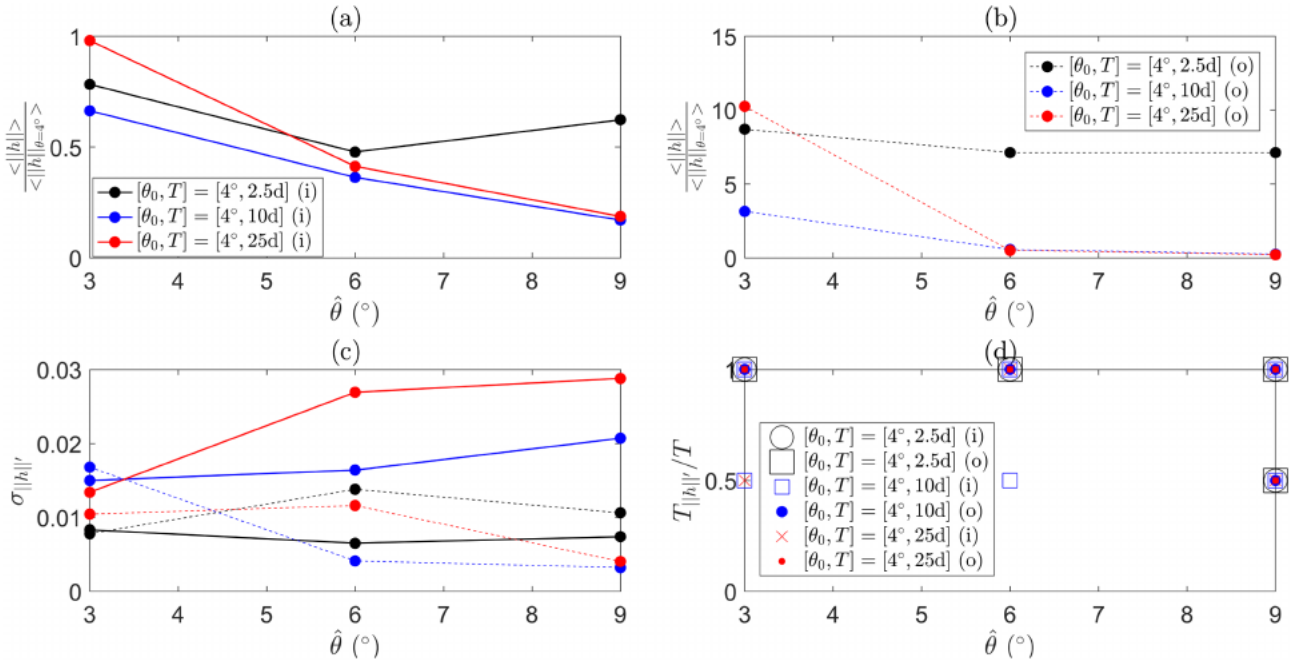

FIGURE 12 As in Figure 7, but in the cases of an oblique mean angle ($\theta_0 = 4°$, Runs7T and Runs8T) [Color figure can be viewed at wileyonlinelibrary.com]

with $C = \alpha/D$ the sediment stirring factor α (defined in Eqs. S12-S13 in the SI) divided by water depth D. Quantity C can be interpreted as a depth-averaged volumetric sediment concentration, which includes both bedload and suspended load. Furthermore, $\Gamma = \alpha\gamma u_{rms}$ is the morphodynamic diffusivity coefficient, with γ the bed slope coefficient and u_{rms} is the near-bed root-mean-square orbital velocity amplitude of the waves (defined in Eq. S11).

A global growth rate σ of bottom perturbations h is defined as

$$\sigma \equiv \frac{1}{||h||^2} h \frac{\partial h}{\partial t}, \tag{7}$$

where the overline " " denotes an averaging over the entire model domain. Using Equation (6), the global growth rate becomes

$$\sigma = \frac{1}{||h||^2}(P_u + P_v - \Delta). \tag{8}$$

In this expression, terms $P_u = -\frac{1}{1-p} hDu\frac{\partial C}{\partial x}$ and $P_v = -\frac{1}{1-p} hDv\frac{\partial C}{\partial y}$ are sources of production of bottom instabilities by cross-shore and longshore processes, respectively. Production term P_u contributes to bar growth, either through the bed-surf coupling mechanism (that is, a positive feedback between the bottom perturbations and the breaking waves, Ribas et al. 2015) in the case of normal and near-normal angles of wave incidence, or through the bed-flow mechanism (that is, a positive feedback between the sea-bed and the alongshore currents, Falqus et al., 1996) in the case of highly oblique angles and the associated strong longshore currents. In the former mechanism, alongshore variations in water depth due to wave breaking over the sand bars induce longshore variations in wave set-up. This forces water to flow alongshore from bar crests to channels (rip feeders). At the latter locations, mass conservation forces the water to move offshore, thereby generating a cross-shore current u. In the latter mechanism, u is induced by the offshore (onshore) deflection of the longshore current over up-current oriented (down-current oriented) bars. Term P_v becomes an important source for bar growth in the case of large wave angles, which result in the generation of strong longshore currents (Thiebot et al., 2012). The diffusive term $\Delta = \frac{1}{1-p} h\vec{\nabla}\cdot(\Gamma\vec{\nabla}h)$, which describes the bed-level changes due to divergence of the downslope gravitational sediment transport, is responsible for damping of bottom instabilities.

For normally incident waves, the production of instabilities is fully governed by term P_u, which arises through the bed-surf coupling mechanism. Bottom perturbations h grow if $P_u > 0$. This means that horns ($h > 0$) grow if u and $\partial C/\partial x$ have opposite signs. The opposite applies for bays ($h < 0$), that is, they grow (i.e., deepen) if u and $\partial C/\partial x$ have the same signs. For obliquely incident waves, term P_v may also contribute to growth of instabilities as a result of a positive feedback between the longshore current v and the bottom perturbations. This requires that v and $\partial C/\partial x$ have opposite signs over the horns and same signs in the bays.

4.2 | Normally incident waves

4.2.1 | Constant angle

It turns out that, in the case of constant wave forcing (Run1), 3D bars first form in the inner domain and subsequently in the outer domain (left panels of Figure 4). Figure 13 shows that a rip-channel system initially develops shoreward of the inner shore-parallel bar (panel a). Rip current u is directed shoreward over the horns and seaward in the bays, while gradient $\partial C/\partial x$ is positive shoreward of the inner shore-parallel bar. This means that growth of this rip-channel system is governed by production term P_u. Weak mirror bottom patterns also appear seaward of this shore-parallel bar, that is, seaward horns (bays) face shoreward bays (horns) (panel b). Over time, 3D bars start to form shoreward (and also seaward) of the outer shore-parallel bar, whose growth is also governed by term P_u (panels c, d).

The merging of seaward inner bars with the shoreward outer bars over time shows that morphodynamic activity in the inner and outer

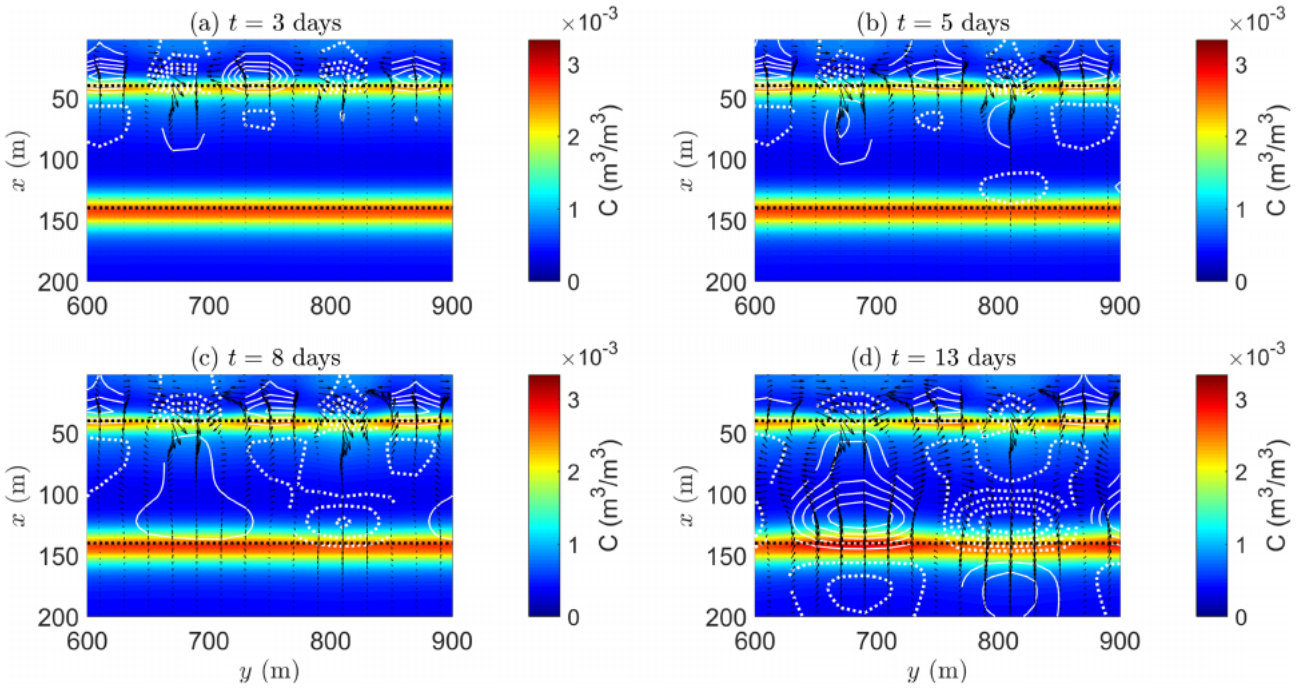

FIGURE 13 Depth-averaged sediment concentration C (m^3/m^3; colours) with superimposed the flow field (arrows) at four different time points during the initial bar growth. Horns (bays) are indicated by the solid (dashed) white contour lines [Color figure can be viewed at wileyonlinelibrary.com]

domains become mutually coupled. This means that the initial formations of inner and outer bars are due to morphodynamic self-organisation, but over time these bars become coupled to each other. Such a transition from free, uncoupled to more forced, coupled behaviour of bottom patterns in the inner domain has indeed been observed in the field (Ruessink et al., 2007). Also, the coupling of inner bars at half the wavelength of outer bars is supported by field observations (Castelle et al., 2007). Results from an additional simulation (not shown), where Run1 was repeated in the absence of the outer shore-parallel bar, show that the wavelength of the 3D bars in the inner domain (about 135 m) differs from that in the case that both inner and outer shore-parallel bars are present (about 125 m). This clearly indicates that the 3D bars in the inner domain are affected by the development of 3D bars in the outer domain such that they become phase-locked. The reason for this particular type of coupling is not fully clear yet. Castelle et al. (2010b) explained that this type of coupling is related with wave focusing in the areas shoreward of the horns of the 3D bars in the outer domain. As a result, two inner rip circulation cells develop between two outer horns, leading to the formation of bars in the inner domain that have half the outer-bar wavelength. However, this does not explain the type of coupling obtained in the present study. This is because (1) waves are not focussed but break over the outer shore-parallel bar (result not shown) and that (2) the 3D bars in the outer domain form as free instabilities, while Castelle et al. (2010b) used pre-existing 3D bars in the outer domain as initial bottom conditions to force their double-barred beach system.

4.2.2 | Time-varying angle

Once the angle of wave incidence varies periodically in time, the 3D bars are much more irregular. They have weaker longshore rhythmicity, irregular longshore pattern migration and their horns and bays merge and split in time (right panels of Figure 4). Although the 3D bars in the outer domain still influence the evolution of those in the inner domain, these bars are no longer phase-locked. This can be explained as follows. During one oscillation period T of the wave angle around a 0-mean, the intensity of rip currents u in the area where the waves break experience alternating time intervals of growth (decreasing wave obliquity) and decay (increasing wave obliquity). Moreover, the correlation between u and bottom perturbations h becomes alternately weaker and stronger when the wave angle increases and decreases, respectively. As a result, production P_u oscillates in time, meaning that inner and outer bars experience alternating growth and decay during one oscillation period. However, bar growth in the inner domain is stronger than that in the outer domain, independently of the wave angle. This can be seen from Figure 14, which shows global growth rate σ (Equation 8) of the inner and outer bars for different (constant) wave angles. The difference between bar growth in the inner and outer domain indicates that the morphodynamic response of outer bars to the continuously changing wave angle is longer than that of the inner bars. Hence, a phase-locked morphological coupling between inner and outer bars cannot be (fully) established. This explains why this type of morphological coupling is not often observed in real beach systems, as these systems are continuously exposed to time-varying wave conditions.

Model results reveal a maximum standard deviation $\sigma_{||h||'}$ of height anomalies $||h||'$ of the inner and outer bars for a forcing period $T = T_a \simeq 15$ days, with T_a the adjustment time scale of the double-barred beach system. This is a resonance feature that is related to the degree of inertia of this system, measured by time scale T_a. If forcing periods $T \sim T_a$, a strong response is possible because the system has ample time to adjust to the forcing. If $T \ll T_a$, the system has no time to respond to the oscillatory forcing and $\sigma_{||h||'}$ will be small, whilst if $T \gg T_a$, the system will experience the time-varying wave angle as if it were constant and $\sigma_{||h||}$ will then scale with the amplitude $\hat{\theta}$ of the

variation in this angle. This reasoning implies that, if $T \ll T_a$, bars in the inner domain would have approximately the same mean height $\langle ||h|| \rangle$ as those in the case of the time-invariant angle. Due to inertia, the double-barred beach system does not have sufficient time to effectively respond to the time-varying wave angle. In the case of single-barred beach system, Nnafie et al. (2020) constructed a similar curve as the ones showed in Figure 14 and found that the mean bar height in the cases of a time-varying wave is the same as that in the case of a time-invariant angle when $T \ll T_a$. In the present study, bars in the inner domain initially do have the same mean height as those of a time-invariant angle (result not shown). However, once 3D bars develop in the outer domain, the mean height of the inner bars decreases. These findings again highlight the large influence of outer bars on the dynamics of inner bars.

Finally, model results show that height anomalies $||h||'$ of inner and outer bars have a dominant response period $T_{||h||'}$ that is half the forcing period T, that is, $T_{||h||'} = T/2$. These results are similar to those of Nnafie et al. (2020) in the case of one single shore-parallel bar. This halving of the response period can be explained based on Figure 14. First, for waves that have a periodically varying angle of incidence around a zero mean, the wave angle obeys $\theta(t) = -\theta(t + T/2)$, that is, half a forcing period later the angle has the opposite sign. Second, growth rates of bars for a constant positive θ are the same as those obtained for the opposite angle $-\theta$. Thus, during one forcing period T, two cycles in the bar growth will occur.

4.3 | Obliquely incident waves

In the case of waves with a constant angle of incidence at the offshore boundary ($\theta = 4^\circ$) with respect to the shore-normal, the left panels of Figure 8 reveal that 3D bars only form in the inner domain.

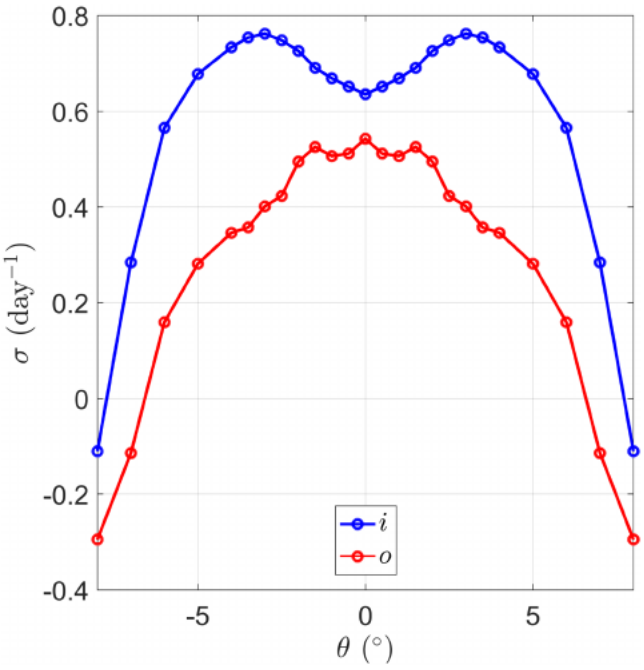

FIGURE 14 Global growth rate σ (Equation 8) of inner (blue) and outer (red) bars for different constant wave angles θ. Growth rate σ is computed over the first 10 days of the simulation period (initial growth) [Color figure can be viewed at wileyonlinelibrary.com]

The low morphodynamic activity in the outer domain is because the waves are too oblique to generate sufficiently strong rip currents when they break over the outer bar, as can be seen from Figure 15a. Therefore, the production of instabilities from cross-shore processes (P_u) is too weak to trigger growth of instabilities in the outer domain. This applies also for the production of instabilities from longshore processes P_v, as a result of a too weak longshore gradient of the concentration $\partial C/\partial y$ (result not shown). Note that the simulations in the present study were restricted to normal and near-normal (mean) wave angles. For these low angles, bed instabilities are fully governed by production term P_u, through the bed-surf coupling mechanism (Section 1). If the intensity of the rip currents u and/or the correlation between u and bottom perturbations h (and thus production term P_u) are too weak, instabilities do not grow. In the present study, instabilities do not grow beyond a critical angle θ_c (~7°). However, an additional simulation for a much larger (constant) wave angle ($\theta = 30^\circ$) showed the development of shore-oblique 3D bars in the outer domain, similar to those obtained by Thiebot et al. (2012) for large angles. For large wave angles term P_v becomes an important source for bar growth as a result of the strong longshore currents (Thiebot et al., 2012). Production term P_u still contributes to bar growth, but it now arises through the offshore meandering of the longshore current over the bar crests (bed-flow mechanism) rather than the bed-surf mechanism.

When wave angle $\theta(t)$ varies about a mean value $\theta_0 = 4^\circ$, 3D bars eventually emerge in the outer domain. This is because, during one oscillation period, there are time intervals when waves are almost normal to the coast. Such conditions result in an increase of the strength of rip currents u and of the correlation between u and bottom perturbations h and thus of production P_u in the outer domain. This is also visible in Figure 15b-e.

The temporal evolution of the bar height is more complicated than in the case of (on average) normally incident waves. The Fourier spectra of the time series of height anomalies $||h||'$ reveal dominant peaks $T_{||h||'}$ at the forcing period ($T_{||h||'} = T$) for both the inner and outer bars. A weak peak at half the forcing period ($T_{||h||'} = T/2$) also appears, particularly in the height anomalies of the inner bars. The occurrence of these dominant peaks at the forcing period is because the growth rates of the bars are asymmetric with respect to the mean angle ($\theta_0 = 4^\circ$), as is seen from Figure 14. Thus, during one forcing period, only one cycle in the bar height will occur. From Figure 14 it further appears that, for wave angles in the range $\theta(t) = [1^\circ, 5^\circ]$, the growth curve of the inner bars is symmetric around $\theta_0 = 3^\circ$. This explains the presence of the weak peak $T_{||h||'} = T/2$ in the time series of height anomalies of these bars.

4.4 | Model limitations

As the overall goal of this study was to gain fundamental insights into the influence of time-varying wave angles on the non-linear dynamics of double-barred beach systems, a highly idealised model (Morfo55) was used and hence it contains several limitations. Some of these limitations are discussed below.

First, field observations (e.g. Almar et al., 2010; Masselink et al., 2014) suggest that bars are strongly affected by tides. This is because they induce time-varying changes in water level, which will

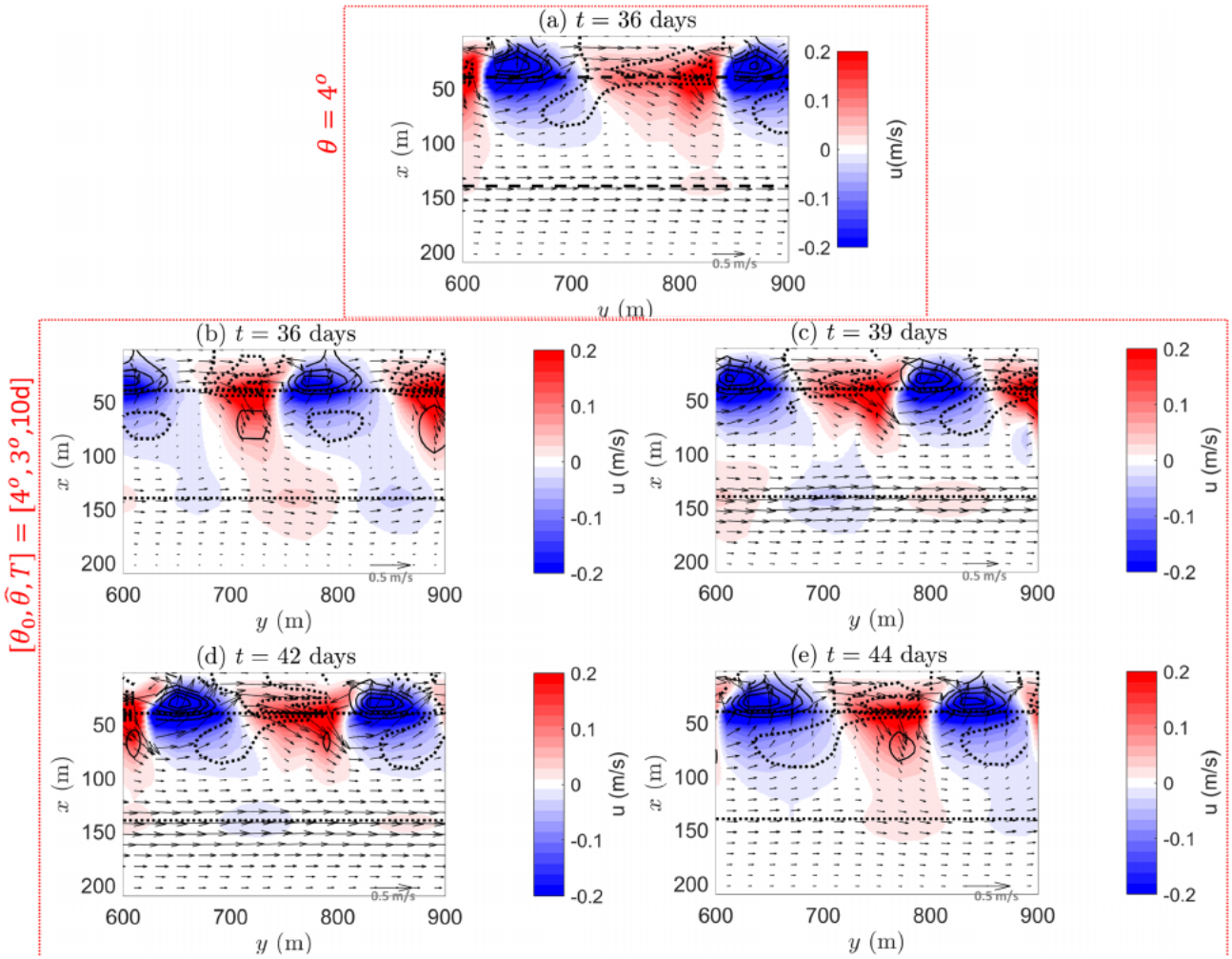

FIGURE 15 (a) Snapshots of the cross-shore velocity component u (colours) with superimposed the flow field (arrows) at $t = 36$ days in the case of Run5 (constant angle $\theta = 4^{\circ}$). Blue and red colours represent, respectively, seaward (shoreward) directed current u. Horns (bays) are indicated by the solid (dotted) black contour lines, while the dashed lines denote the locations of the inner and outer shore-parallel bars. (b-e) As in (a), but showing snapshots in the case of Runs6T (time-varying wave angle around $\theta = 4^{\circ}$, with amplitude $\hat{\theta} = 3^{\circ}$ and period $T = 10$ days) at four different time points during one oscillation period [Color figure can be viewed at wileyonlinelibrary.com]

continuously change wave breaking and refraction across the shore-parallel bars. Walstra et al. (2012) found that higher water levels promote bar growth when the wave angle is large ($\theta > 20^{\circ}$), suggesting that tides may have a strong impact on the bar dynamics. As the present study is limited to normal and near-normal (mean) wave angles, tides are not expected to fundamentally change the present outcomes. The latter is also confirmed by Price et al. (2013), who modelled the morphodynamic response of a double-bar system to waves with angles $\theta < 20^{\circ}$. They found that the inclusion of tides weakens the growth of bars, but it did not qualitatively change their overall dynamics.

Second, Morfo55 assumes waves to have a narrow spectrum in both their frequency and angle. Nnafie et al. (2020), who used Morfo55 to study the response of a single-barred beach system to time-varying wave angles, reported quantitative differences between their simulated bar heights and those obtained by Castelle and Ruessink (2011). Nnafie et al. (2020) argued that the use of the spectral wave model SWAN by Castelle and Ruessink (2011) could explain these differences. This aspect requires further study.

Third, to simplify the analysis, the configuration of the inner and outer shore-parallel bars (amplitude, depth, distance between the bars, etc.) was kept constant in the present study. A merging of seaward inner 3D bars with shoreward outer ones was observed in Figure 13. This merging raises the question of to what extent the presence of 3D bars in the inner domain influences the morphodynamic activity in the outer domains. According to Thiebot et al. (2012), the influence is one way, meaning that dynamics of 3D bars in the inner domain do not influence those in the outer domain. However, results from an additional simulation where Run1 was repeated in the absence of the inner shore-parallel bar (constant wave angle) reveal that, in this case, 3D bars in the outer domain grow less rapidly and become higher than those of Run1 (Figure SI-9). Their wavelength does not change. This means that the coupling between inner and outer 3D bars works both ways. This two-way morphological coupling between inner and outer bars might be due to the different configuration of the shore-parallel bars used by Thiebot et al. (2012). For example, an outer shore-parallel bar that is located in deeper water, as is the case in the model configuration of Thiebot et al. (2012), is expected to be less affected by the flow circulation near the inner shore-parallel bar. Meanwhile, the outer shore-parallel bar can still influence the shoreward propagation of the waves through for example changes

in refraction and breaking patterns. This will affect the flow patterns and thus the dynamics of the 3D bars in the inner domain. Double-barred beach dynamics for different bar configurations is a key topic of future research.

Fourth, the growth rate curves shown in Figure 14 suggest that bars do not grow beyond a critical angle $\theta = 7^{\circ}$, similar to the situation of a single-barred beach system (Garnier et al., 2008; Nnafie et al., 2020). However, as mentioned in the previous section, shore-oblique 3D bars grow for a much larger angle ($\theta = 30^{\circ}$), whose growth is governed by both P_u and P_v (Garnier et al., 2006; Thiebot et al., 2012). Further research is needed to assess how a time-varying wave angle would influence this type of bars.

Sixth, in all the simulations, random bottom perturbations ('white noise') with an amplitude of 2.5 cm were superimposed on the initial bathymetry to trigger the self-organisation processes. Nnafie et al. (2020), who also used the model Morfo55 to study the impact of a time-varying wave angle on the non-linear evolution of a single barred-beach system, found that using different initial bottom perturbations (random perturbations, hump of sand, longshore periodic bars) did not change their model results. In all the different cases, the bars have the same characteristics (i.e., same spatial patterns, height and migration) during their non-linear evolution, although these characteristics may differ during their initial formation. As the focus of the present study is mainly on the non-linear evolution of the bars, it is expected that the present results will remain robust to using other initial bottom perturbations.

Seventh, observations show that bars often experience a net offshore/onshore directed migration (Gallagher et al., 1998; Wijnberg & Terwindt, 1995; Winant et al., 1975). This feature is not captured by the present model, which is attributed to the fact that the model does not resolve vertical processes. Examples of these processes include (1) the onshore sediment transport due to wave non-linearities (associated with velocity and acceleration skewness) and wave streaming and (2) the offshore transport due to undertow (Elgar et al., 2001; Gallagher et al., 1998). These processes have been studied by using various types of cross-shore profile models (Fernndez-Mora et al., 2015; Hsu et al., 2006; Walstra et al., 2012). Indeed, such models are able to simulate observed onshore/offshore migration, but they do not account for longshore variations. Dubarbier et al. (2017), who parametrised the effects of wave non-linearities and undertow on the sediment transport in a 2DH numerical model, were able to simulate both the cross- and longshore bar migrations. The incorporation of vertical processes in the Morfo55 model would be an interesting addition, particularly when considering alternating high and low energetic wave events that generally induce offshore and onshore sediment transport, respectively.

Finally, when mature 3D bars develop in the inner and outer domain, they interact with each other such that their heights increase in time, without reaching a dynamic equilibrium state. Apparently, damping of growth of bottom perturbations h (term Δ in Equation 8) is not strong enough to oppose this additional growth of the bars. This ultimately leads to model blow-up. It would be interesting to implement potential processes that could prevent this, such as drying/flooding and adding the effect of wave rollers, also in sediment transport.

5 | CONCLUSIONS

This study has addressed the response of a modelled double-barred beach system to periodically time-varying wave angles. The parameters have been chosen such that the cross-shore beach profile crudely represents that of the Gold Coast, Australia. The main findings are listed below.

When waves are normally incident to the coast ($\theta = 0^{\circ}$), alongshore rhythmic 3D bars first emerge in the inner domain, whose growth is governed by morphodynamic self-organisation. In the course of time, 3D bars also develop in the outer domain, which influence the bar dynamics in the inner domain (forced behaviour). The inner bars also influence the bar dynamics in the outer domain. Eventually, a bottom pattern forms where the inner bars are coupled at half the wavelength of the outer bars (phase-locked). When the wave angle varies around a 0-mean angle ($\theta_0 = 0^{\circ}$), the 3D bars in the inner and outer domains still interact with each other. However, these bars are no longer phase-locked. Moreover, in this case, the 3D bars are more irregular, that is, they are less rhythmic in the longshore direction and their horns and bays merge and split over time.

When the waves have a constant oblique angle of incidence ($\theta = 4^{\circ}$), 3D bars grow only in the inner domain. Their heights saturate during their non-linear evolution and they do not migrate in the direction of the longshore current. The morphodynamic activity in the outer domain is rather weak. When the wave angle varies around an oblique mean angle $\theta_0 = 4^{\circ}$, 3D bars initially emerge only in the inner domain. Over time, 3D bars also develop in the outer domain. Prior to the formation of the latter bars, the inner bars have a distinct wavelength, their heights reach a dynamical equilibrium and they have a regular migration in the downstream direction. Once 3D bars grow in the outer domain, this regular evolution of the inner bars is disrupted. They become less rhythmic, their heights start to increase and their migration seems to follow the rapidly migrating outer bars.

When the wave angle varies in time, the 3D bars that develop in the inner and outer domain have heights that also oscillate in time. On average, the heights of the inner and outer bars are, respectively, smaller and larger than their corresponding heights in the case of a time-invariant angle. The oscillations in the bar heights reach a maximum when the forcing period in the wave angle is comparable to the adjustment time scale of the system (about 10-20 days). For a time-varying wave angle around a 0-mean, the height oscillations have dominant peaks at half the forcing period. For a time-varying angle around an oblique mean, these oscillations have dominant peaks at the forcing period. Also in this case, there are weaker peaks at half the forcing periods in the height oscillations of the inner bars.

Increasing the amplitude of the angle variation weakens the growth of 3D bars in the inner and outer domain, particularly when the waves have (on average) an oblique mean and the period of their oscillations is of the order of the system adjustment time scale.

CONFLICT OF INTEREST STATEMENT

The authors declare that there are no conflicts of interest.

DATA AVAILABILITY STATEMENT

The data that support the findings of this study are available from the corresponding author upon reasonable request.

ORCID

A. Nnafie https://orcid.org/0000-0002-4459-5427

T.D. Price https://orcid.org/0000-0003-3664-4417

REFERENCES

Almar, R., Castelle, B., Ruessink, B.G., Sénéchal, N., Bonneton, P. & Marieu, V. (2010) Two- and three-dimensional double-sandbar system behaviour under intense wave forcing and a meso-macro tidal range. *Continental Shelf Research* 30, 781–792.

Bashforth, F. & Adams, J. (1883) *An attempt to test the theories of capillary action by comparing the theoretical and measured forms of drops of fluid*. Cambridge University Press: Cambridge.

Calvete, D., Coco, G., Falqués, A. & Dodd, N. (2007) Morphological development of rip channel systems: Normal and near-normal wave incidence. *Geophysical Research Letters* 34, L05605.

Calvete, D., Dodd, N., Falqués, A. & Van Leeuwen, S.M. (2005) (un)predictability in rip channel systems. *Journal of Geophysical Research* 110, C10006.

Castelle, B., Bonneton, P., Dupuis, H. & Senechal, N. (2007) Double bar beach dynamics on the high-energy meso-macrotidal French Aquitanian Coast: A review. *Marine Geology* 245, 141–159.

Castelle, B. & Ruessink, B.G. (2011) Modeling formation and subsequent nonlinear evolution of rip channels: Time-varying versus time-invariant wave forcing. *Journal of Geophysical Research: Earth Surface* 116(F4), F04008.

Castelle, B., Ruessink, B.G., Bonneton, P., Marieu, V., Bruneau, N. & Price, T.D. (2010a) Coupling mechanisms in double sandbar systems. part 2: Impact on alongshore variability of inner-bar rip channels. *Earth Surface Processes and Landforms* 35, 771–781.

Castelle, B., Ruessink, G., Bonneton, P., Marieu, V., Bruneau, N. & Price, T. (2010b) Coupling mechanisms in double sandbar systems. part 1: Patterns and physical explanation. *Earth Surface Processes and Landforms* 35, 476–468.

Coco, G., Calvete Manrique, D., Ribas, F., de Swart, H. & Falqués, A. (2020) Emerging crescentic patterns in modelled double sandbar systems under normally incident waves. *Earth Surface Dynamics* 8, 323–334.

Deigaard, R., Drønen, N., Fredsøe, J., Jensen, J.H. & Jørgensen, M.P. (1999) A morphological stability analysis for a long straight barred coast. *Coastal Engineering* 36, 171–195.

Dubarbier, B., Castelle, B., Ruessink, G. & Marieu, V. (2017) Mechanisms controlling the complete accretionary beach state sequence. *Geophysical Research Letters* 44(11), 5645–5654.

Elgar, S., Gallagher, E.L. & Guza, R.T. (2001) Nearshore sandbar migration. *Journal of Geophysical Research: Oceans* 106(C6), 11623–11627.

Falqus, A., Montoto, A. & Iranzo, V. (1996) Bed-flow instability of the longshore current. *Continental Shelf Research* 16(15), 1927–1964.

Fernndez-Mora, A., Calvete, D., Falqus, A. & de Swart, H.E. (2015) Onshore sandbar migration in the surf zone: New insights into the wave-induced sediment transport mechanisms. *Geophysical Research Letters* 42(8), 2869–2877.

Gallagher, E.L., Elgar, S. & Guza, R.T. (1998) Observations of sand bar evolution on a natural beach. *Journal of Geophysical Research: Oceans* 103(C2), 3203–3215.

Garnier, R., Calvete, D., Falqués, A. & Caballeria, M. (2006) Generation and nonlinear evolution of shore-oblique/transverse sand bars. *Journal of Fluid Mechanics* 567, 327–360.

Garnier, R., Calvete, D., Falqués, A. & Dodd, N. (2008) Modelling the formation and the long-term behavior of rip channel systems from the deformation of a longshore bar. *Journal of Geophysical Research* 11, C07053.

Garnier, R., Falqus, A., Calvete, D., Thibot, J. & Ribas, F. (2013) A mechanism for sandbar straightening by oblique wave incidence. *Geophysical Research Letters* 40(11), 2726–2730.

Hsu, T.-J., Elgar, S. & Guza, R.T. (2006) Wave-induced sediment transport and onshore sandbar migration. *Coastal Engineering* 53(10), 817–824.

Jackson, D. & Short, A. D. (eds). (2020) *Sandy beach morphodynamics*. Elsevier.

Klein, M. & Schuttelaars, H.M. (2006) Morphodynamic evolution of double-barred beaches. *Journal of Geophysical Research* 111, C06017.

Komar, P.D. (1998) *Beach processes and sedimentation*. Prentice-Hall.

Lippmann, T.C. & Holman, R.A. (1990) The spatial and temporal variability of sand bar morphology. *Journal of Geophysical Research: Oceans* 95(C7), 11575–11590.

Masselink, G., Austin, M., Scott, T., Poate, T. & Russell, P. (2014) Role of wave forcing, storms and NAO in outer bar dynamics on a high-energy, macro-tidal beach. *Geomorphology* 226, 76–93.

Nnafie, A., van Andel, N. & de Swart, H. (2020) Modelling the impact of a time-varying wave angle on the nonlinear evolution of sand bars in the surf zone. *Earth Surface Processes and Landforms* 45(11), 2603–2612.

Price, T.D., Castelle, B., Ranasinghe, R. & Ruessink, G. (2013) Coupled sandbar patterns and obliquely incident waves. *Journal of Geophysical Research: Earth Surface* 118, 1677–1692.

Price, T.D. & Ruessink, B. G. (2013) Observations and conceptual modelling of morphological coupling in a double sandbar system. *Earth Surface Processes and Landforms* 38(5), 477–489.

Price, T.D., Ruessink, G. & Castelle, B. (2014) Morphological coupling in multiple sandbar systems: a review. *Earth Surface Dynamics* 2, 309–321.

Ribas, F., Falqués, A., de Swart, H.E., Dodd, N., Garnier, R. & Calvete, D. (2015) Understanding coastal morphodynamic patterns from depth-averaged sediment concentration. *Reviews of Geophysics* 53, 362–410.

Ruessink, G., Coco, G., Ranasinghe, R. & Turner, I. (2007) Coupled and noncoupled behavior in double sandbar morphology. *Journal of Geophysical Research* 112, 125–129.

Smit, M.W.J., Reniers, A.J.H.M., Ruessink, B.G. & Roelvink, J.A. (2008) The morphological response of a nearshore double sandbar system to constant wave forcing. *Coastal Engineering* 55(10), 761–770.

Soulsby, R. (1997) *Dynamics of marine sands: a manual for practical applications*. Thomas Telford.

Thiebot, J., Idier, D., Garnier, R., Falqués, A. & Ruessink, G. (2012) The influence of wave direction on the morphological response of a double sandbar system. *Continental Shelf Research* 32, 71–85.

van Enckevort, I.M.J., Ruessink, B.G., Coco, G., Suzuki, K., Turner, I.L., Plant, N.G. & Holman, R.A. (2004) Observations of nearshore crescentic sandbars. *Journal of Geophysical research* 109, C06028.

van Enckevort, I.M.J. & Wijnberg, K.M. (1999) Intra-annual changes in bar plan shape in a triple bar system, Coastal sediments, ASCE.

Walstra, D.J.R., Reniers, A.J.H.M., Ranasinghe, R., Roelvink, J.A. & Ruessink, B.G. (2012) On bar growth and decay during interannual net offshore migration. *Coastal Engineering* 60, 190–200.

Wijnberg, K.M. & Terwindt, J.H.J. (1995) Extracting decadal morphological behaviour from high-resolution, long-term bathymetric surveys along the Holland coast using eigenfunction analysis. *Marine Geology* 126(1), 301–330.

Winant, C.D., Inman, D.L. & Nordstrom, C.E. (1975) Description of seasonal beach changes using empirical eigenfunctions. *Journal of Geophysical Research (1896-1977)* 80(15), 1979–1986.

Wright, L.D. & Short, A.D (1984) Morphodynamic variability of surf zones and beaches: a synthesis. *Marine Geology* 56(1-4), 93–118.

Yu, J. & Slinn, D.N (2003) Effects of wave-current interaction on rip currents. *Journal of Geophysical Research: Oceans* 108(C3), 3088.

SUPPORTING INFORMATION

Additional supporting information may be found online in the Supporting Information section at the end of this article.

How to cite this article: Nnafie, A, Driessen, AS, de Swart, HE, Price, TD. Modelling the response of a double-barred sandy beach system to time-varying wave angles. *Earth Surf. Process. Landforms*. 2021;46:1393–1409. https://doi-org.proxy.library.uu.nl/10.1002/esp.5107